Wind and Phytoplankton Dynamics Drive Seasonal and Short-Term Variability of Suspended Matter in a Tidal Basin

**Gaziza Konyssova[1,2*], Vera Sidorenko[1,2], Alexey Androsov[1,2], Sabine Horn[2], Sara Rubinetti[1,3],
Ivan Kuznetsov[1], Karen Helen Wiltshire[2,4], Justus van Beusekom[2,5]**

[1] Alfred-Wegener-Institut Helmholtz-Zentrum für Polar- und Meeresforschung, Bremerhaven, Germany
[2] Wadden Sea Station Sylt, Alfred-Wegener-Institut Helmholtz-Zentrum für Polar- und
Meeresforschung, List/Sylt, Germany
[3] Dipartimento per lo Sviluppo Sostenibile e la Transizione Ecologica, University of Piemonte
Orientale, Vercelli, Italy
[4] Climate Science Trinity College Dublin, Dublin, Ireland
[5] Institute for Carbon Cycles, Helmholtz Centre Hereon, Geesthacht, Germany

* Correspondence:
Gaziza Konyssova
gaziza.konyssova@awi.de
ORCID: 0009-0008-5460-4754

Abstract
Suspended particulate matter (SPM) is a key component of coastal ecosystems, modulating light
availability, nutrient transport, and food web dynamics. Its variability is driven by a combination of
physical and biological processes that interact across temporal and spatial scales. Using the Sylt-Rømø
Bight as a natural laboratory and focusing on the period 2000-2019, in this study, we integrate statistical
analysis of observational data from the Sylt Roads monitoring program and local meteorological
stations, neural network modelling and Lagrangian transport simulations. This multi-method approach
enables us to disentangle and quantify the relative roles of tidal and wind forcing, as well as biological
processes in shaping SPM concentrations across various time scales, based on near-surface
measurements at two monitoring stations.
The findings show that wind intensity dominates short-term SPM variability, particularly at the shallow
station, where SPM responds rapidly to local wind-induced resuspension. At the deep station, the wind
effects appear with a delay of ~5 days, aligning with tidally induced transport timescales (~133 hours)
from shallower resuspension zones, as revealed by Lagrangian simulations. Seasonal patterns are
further modulated by both reduced wind intensities and the onset of biological processes, such as
phytoplankton blooms, which promote flocculation and subsequent settling in spring and summer.
Neural network experiments highlight the shifting seasonal balance between physical and biological
controls. The median concentration of SPM decreased by up to 80% from winter to summer.
Approximately 40% of this seasonal difference can be attributed to weaker wind conditions, while the
remaining ~40% is likely driven by biologically mediated sinking processes.

1 Introduction

Suspended particulate matter (SPM) is a key component of coastal systems, influencing a wide range of physical and ecological processes. It consists of a mixture of small solid particles of both organic and inorganic origin suspended in the water column with concentrations, size (Eisma, 1986) and composition varying spatially and temporally (Schartau et al., 2019). The spatiotemporal variation in SPM concentrations is driven by an interplay of hydrodynamic, meteorological, and biological factors, which in turn, regulate nutrient availability, light penetration, and organic matter distribution. This directly impacts ecosystem productivity, including the timing of the phytoplankton bloom in spring (Cadée, 1986) and spatial gradients in primary productivity (Cloern, 1987; Colijn, 1982), and trophic interactions (Dolch and Reise, 2010; Graf and Rosenberg, 1997).

In tidally energetic environments like the Wadden Sea, the suspended matter gradient is kept upright by the density-driven coastward transport of bottom water and tidal straining (Becherer et al., 2016; Burchard et al., 2008; Flöser et al., 2011). Sediment accumulation is further influenced by hydrodynamic retention mechanisms such as enhanced settling due to the landward dissipation of current velocity, the scour-lag (Dyer, 1995; Friedrichs and Aubrey, 1988) and settling lag effects (Postma, 1967), and the tidal asymmetry formed by the presence of non-linear processes within the tidal system (Dronkers, 1986; Fofonova et al., 2019; Friedrichs and Aubrey, 1988; Hagen et al., 2022). The role of tidal currents in the variability of SPM concentrations is found to be significant through transport processes (Bartholomä et al., 2009; Christiansen et al., 2006) as well as sediment erosion even under calm and moderate weather conditions (Bartholomä et al., 2009; Lettmann et al., 2009). While tides regulate advection and maintain a baseline shear stress, the co-occurrence of strong winds and wave-induced turbulence during severe weather further enhances bottom stress and promotes additional erosion.

Wind stress and wave action are critical in short-term SPM dynamics. Wind-induced resuspension, particularly in shallow coastal areas, causes episodic increases in turbidity (Aarup, 2002; Fettweis et al., 2012). Stronger and more persistent wind forcing during winter maintains higher SPM concentrations, keeping fine sediments in suspension (de Jonge and van Beusekom, 1995; van Beusekom et al., 1999), while calmer conditions in summer enable enhanced settling (Bale et al., 1985; Verney et al., 2009). Beyond physical resuspension and transport mechanisms, biochemical processes also influence SPM concentrations by modulating aggregation, stabilization, and vertical flux of particulate matter (de Jonge and van Beusekom, 1995; van Beusekom and de Jonge, 2002; Verney et al., 2009). For example, flocculation, the aggregation and breakup of particles, is a key mechanism by which biological activity modulates SPM concentrations (Wotton, 2004; Eisma, 1986). Phytoplankton blooms in spring and summer can promote flocculation, leading to enhanced particle settling and reduced SPM concentrations in the water column (de Jonge & van Beusekom, 1995; Schartau et al., 2019). The process is particularly enhanced by the occurrence of extracellular polymeric substances (EPS), including marine gels such as transparent exopolymeric particles (TEPs), but can also occur due to cohesive properties of fine-grained minerals like clays (Passow, 2002; Verney et al., 2009). The size and cohesiveness of these biologically mediated flocs also govern their settling velocities and resuspension thresholds, affecting how quickly particles are redistributed in the water column. Warmer temperatures also accelerate the decomposition of organic matter (OM), which is nearly always present

in natural flocs in various forms (detritus, adsorbed OM molecules, and living OM), and may range from a minor to a dominant fraction of total floc mass (Eisma, 1986; Engel and Schartau, 1999). This directly links SPM dynamics to food-web functioning (Wotton, 2004; Engel & Schartau, 1999). In addition, temperature also affects top-down controls such as zooplankton grazing, which alters SPM composition and concentration through multiple pathways. Grazing modifies the SPM field not only through phytoplankton consumption but also via the fragmentation of aggregates, production of fecal pellets and organic material that promote microbial and TEP-mediated aggregation. The effects of these processes can either promote particle settling or enhance recycling and suspension, depending on community composition, feeding modes, and environmental conditions (e.g., Passow, 2002; Toullec et al., 2019; Turner, 2002).

In the shallow coastal systems, light can reach the seafloor, stimulating benthic algae growth, provided water clarity allows sufficient light penetration (Loebl et al., 2007). These benthic processes further influence SPM concentrations through both stabilization and removal mechanisms. While microphytobenthos, consisting of benthic diatoms and cyanobacteria, produce biofilms that stabilize sediments and reduce resuspension (Stal, 2010), filter-feeding organisms, such as mussels (*Mytilus edulis*) and oysters (*Magallana gigas*), alter SPM dynamics by removing fine particles from suspension, affecting both sediment deposition rates and nutrient cycling (Graf and Rosenberg, 1997). Moreover, excessive nutrient loads can enhance phytoplankton blooms, whose decay products and extracellular polymeric substances facilitate biomineral floc formation (Passow, 2002; van Beusekom et al., 1999), which promotes OM sedimentation and alters benthic-pelagic coupling by influencing the availability of organic matter to both suspension and deposit feeders. These processes collectively shape coastal sediment dynamics, contributing to the long-term evolution of tidal flat environments.

While hydrodynamic and wind-driven influences on SPM have been extensively studied, their interaction with biological processes and relative contributions remain incompletely understood, despite growing interest. By leveraging long-term ecological monitoring data from the Sylt Roads program, this study aims to quantify the contributions of tidally induced and wind-driven resuspension and transport, as well as biologically mediated processes, to the spatiotemporal variability of SPM in the Sylt-Rømø Bight.

This analysis integrates high-resolution in situ measurements from two Long-Term Ecological Research (LTER) stations from 2000 to 2019, meteorological data from the station List (Sylt, Germany), and outputs from hydrodynamic and neural network modelling to evaluate SPM dynamics across short-term (hourly to daily) and seasonal timescales. The following research questions guide the study: (1) What are the dominant mechanisms driving SPM variability across different temporal scales? (2) How do these mechanisms differ between the two monitoring stations within the Sylt-Rømø Bight? (3) How important are biological processes in shaping observed SPM concentrations?

2 Data and Methods

2.1 Area Description

The investigations were carried out in the Sylt-Rømø Bight, a shallow, tidal basin in the northern Wadden Sea (southeastern North Sea; see Fig. 1). The basin is semi-enclosed due to two causeways at its northern and southern ends, isolating it from neighboring basins. Its only connection to the North Sea is through the deep tidal inlet Lister Deep, between the islands of Sylt and Rømø. The bay spans approximately 410 km² and features a highly variable topography, including extensive intertidal flats (>45%), shallow subtidal zones (~35%), and deep tidal channels (~10%). The Sylt-Rømø Bight's bathymetry is characterised by a mean water depth of approximately 4 m, with a maximum depth of about 37 m observed in the tidal inlet Lister Deep. Most subtidal and ~72% of intertidal sediments are sand-dominated. The basin also features a small sheltered embayment Königshafen, with an average depth of ~2m and encompasses large areas which become exposed at low tides.

The tidal range in the bight averages 2 m, based on observations at the List tide gauge (E.U. Copernicus Marine Service Information, doi.org/10.48670/moi-00036). Tidal forcing accounts for over 80% of depth-averaged velocity variability under regular wind conditions, in the absence of storms, and over 90% during spring tides (Fofonova et al., 2019). The bight receives minimal fluvial input, with small rivers such as the Vidå and Brede Å (see Fig.1), contributing only 4–10 m³/s of freshwater (Purkiani et al., 2015). Water exchange with the open North Sea occurs exclusively through Lister Deep, a 2.8 km wide tidal inlet. At the mouth of Lister Deep, a prominent ebb-tidal delta extends seaward, acting as both a sediment trap and a pathway for sediment redistribution within the bight (Dissanayake et al., 2012). Localized anthropogenic disturbance may also influence sediment availability and distribution in the region, although detailed records of maritime traffic, dredging operations, and benthic trawling specific to the Sylt-Rømø Bight are limited. However, studies from the broader Wadden Sea show that anthropogenic activities such as bottom trawling (e.g., Bruns et al., 2023; Depestele et al., 2016), dredging (de Jonge and de Jong, 2002; de Jonge, 1983; van Maren et al., 2015), and mussel farming (Jansen et al., 2023) are recognized drivers of sediment disturbance and resuspension.
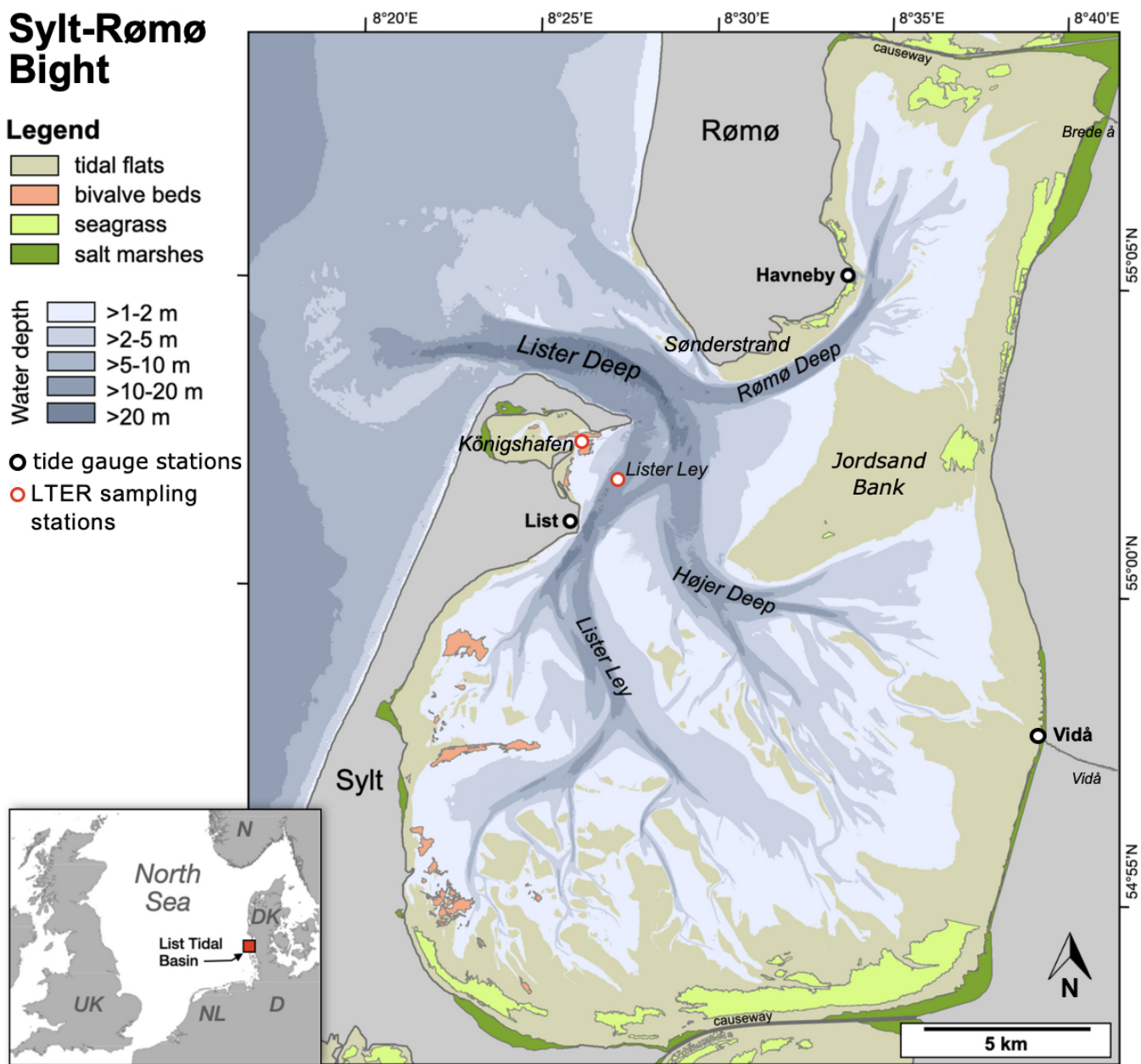
Figure 1: Map of the Sylt-Rømø Bight showing bathymetry, key habitats (tidal flats, bivalve beds, seagrass meadows, and salt marshes), LTER sampling stations (Deep Station – Lister Ley; Shallow Station – Königshafen), tide gauge locations (List, Havneby, Vidå), and rivers (Brede Å and Vidå). The basin is connected to the North Sea via the tidal inlet Lister Deep and laterally enclosed by causeways to the north and south.

2.2 FESOM-C Model

This study used the coastal hydrodynamic model FESOM-C (Androsov et al., 2019). FESOM-C is designed explicitly for high-resolution coastal applications and employs a finite-volume cell-vertex

5

146 discretization on unstructured meshes composed of triangles and quadrilaterals. This allows for flexible
147 spatial resolution down to several metres, suitable for simulating complex coastal dynamics (Fofonova
148 et al., 2019; Kuznetsov et al., 2020, 2024; Neder et al., 2022; Sprong et al., 2020; Sidorenko et al.,
149 2025).

2.2.1 Model Setup

151 The setup utilized an unstructured hybrid mesh of 208,345 nodes and 211,545 elements. Due to the
152 semi-enclosed state of the bight, the mesh contains a single open boundary at the seaward edge of the
153 domain, connecting the basin with the North Sea. The horizontal spatial resolution varies from up to 2
154 m in wetting-drying zones to 304 m in the deeper outer part (near the open boundary). The experiments
155 were carried out by running 2D barotropic simulations with the wetting/drying option enabled to
156 capture the periodic submergence and exposure of intertidal areas. The model timestep was set to ~ 0.25
157 seconds, with data output every ~20 minutes of simulation time. The bottom friction coefficient was
158 applied as 0.0025, a value identified as optimal in prior studies of the same study area when using
159 TPXO9 tidal solution (Fofonova et al., 2019; Konyssova et al., 2025).
160 The simulations are driven by tidal forcing alone, applied at the open boundary. For an accurate
161 simulation of the tidal dynamics, thirteen major tidal harmonic constituents (M2, S2, N2, K2, K1, O1,
162 P1, Q1, Mm, Mf, MN4, 2N, and S1) and two over-harmonics (M4, MS4) were prescribed by their
163 phases and amplitudes at the open boundary based on TPXO9 tidal atlas (Egbert and Erofeeva, 2002).
164 This selection of the tidal solution was justified by its robust performance and is one of the most
165 optimal for the North Sea (Fofonova et al., 2019). The current setup has been validated in a previous
166 work by Konyssova et al. (2025). The model's performance has been validated using tidal gauge (TG)
167 data from stations List, Vidå, and Havneby (see Fig. 1; performance results are provided in the
168 Supplementary Materials, Table S1). Since the numerical setup remains unchanged, we refer to
169 Konyssova et al. (2025) for full validation details.

2.2.2 Lagrangian Module

171 To assess tidally driven spatial connectivity and transport timescales within the basin, we performed
172 Lagrangian simulations using FESOM-C Drift, a post-processing tool designed for particle tracking.
173 The model advects massless passive particles based on the velocity fields produced by the
174 hydrodynamic model. In this study, we use the term "passive tracers" to denote Lagrangian particles
175 without weight or settling properties. This is equivalent to virtual Lagrangian particles commonly
176 applied in particle tracking studies and should not be confused with dye experiments that represent
177 concentration changes in space and time.
178 The experiment involved releasing passive tracers from all grid elements within the domain that are
179 consistently inundated during every flood phase. We released about 90,000 tracers at three-hour
180 intervals over six weeks (169 iterations in total). Each tracer was tracked for up to three weeks and was
181 removed from the simulation once it reached either of the two Sylt Roads sampling stations (see Fig. 1
182 and Section 2.3.1). The iterative release process was designed to capture the full range of tidal
183 conditions and the complexity of hydrodynamic transport within the basin, ensuring that the results are

184 statistically robust. Upon arrival at a station, tracers were immediately removed to prevent post-arrival
185 movements from influencing the mapped source regions and transport pathways. The simulations were
186 conducted independently for each station, focusing exclusively on the paths from the release locations
187 to the respective sampling site. If a tracer did not reach the designated station within the simulation time
188 frame, it was considered to originate from a region that falls outside the station's dominant transport
189 pathways.
190 The first analysis approach assessed the source regions of passive tracers arriving at the sampling
191 stations. This allows us to evaluate the connectivity between different subareas of the basin and the
192 sampling sites. The probability of SPM originating from a given area was mapped based on the
193 cumulative occurrence of tracer pathways across all iterations. Higher probability values indicate areas
194 that more frequently serve as source regions or transport pathways for SPM reaching the sampling
195 stations.
196 The second part of the analysis was conducted to estimate the mean transit time of the tracers reaching
197 the sampling stations from shallow source zones, where resuspension typically occurs (defined here as
198 areas <2 m deep, based on de Jonge & van Beusekom, 1995). The mean transit time over all
199 implementations was calculated for all elements whose tracers reached the stations within the simulated
200 three weeks. To quantify how long it typically takes for high tracer concentrations to reach the station,
201 we computed a probability-weighted median transit time, where mean transit times were weighted by
202 their probability values. This approach ensures that frequent transport pathways are given greater
203 influence in the median transit time calculation, reducing bias from rare, low-probability trajectories.

204 **2.3 Data**

205 **2.3.1 Biogeochemistry data**

206 This study used data from the Sylt Roads long-term ecological monitoring program, focusing on a
207 subset from 2000 to 2019 to ensure consistent methodology and regular sampling. From a broad range
208 of hydrographic and biogeochemical parameters covered in the dataset, this study specifically analyzed
209 suspended particulate matter (SPM; mg/L, filtered through 0.4 µm nucleopore filters, rinsed with
210 distilled water, stored frozen, and dried at 60 °C) and chlorophyll-a (Chl-a; µg/L, filtered through GF/C
211 filters (Whatman), stored at −20 °C, and extracted using 90% acetone and analyzed
212 spectrophotometrically using the trichromatic method as described by Jeffrey and Humphrey, (1975).
213 Both parameters were measured twice weekly at a sampling depth of 1 m below the surface at two
214 primary stations: the deep station at the Lister Ley channel and the shallow station at the entrance of
215 Königshafen embayment (see Fig. 1). The full dataset is publicly available on the data portal
216 PANGAEA (https://www.pangaea.de) and the recent evaluation is detailed in Rick et al. (2023).
217 To analyze seasonal variability, we defined the seasons based on observed cycles in Chl-a
218 concentrations at the study site, rather than calendar or astronomical definitions. Specifically, we used:
219 - winter (November 20 – February 19, low biological activity, low Chl-a);
220 - spring (February 20 – May 31, phytoplankton bloom initiation and peak);
221 - summer (June 1 – September 19, post-bloom conditions, high light, reduced Chl-a);
222 - autumn (September 20 – November 20, transitional period).

2.3.2 Meteorological data

For the statistical analysis, we also downloaded the quality checked historical meteorological data for station 3032, List auf Sylt, from Climate Data Center (CDC) of the Deutscher Wetterdienst (DWD). The data includes hourly mean wind speed and wind direction (dataset ID: urn:x-wmo:md:de.dwd.cdc::obsgermany-climate-hourly-wind), and daily sunshine duration (dataset ID: urn:wmo:md:de-dwd-cdc:obsgermany-climate-daily-kl).

2.3.3 Sea Surface Height data

Using the validated model setup (Fofonova et al., 2019; Konyssova et al., 2025), the sea surface height (SSH) data were reconstructed for the deep and shallow stations. In particular, the amplitudes and phases of the 15 harmonics mentioned above were obtained from the modeling output using Fast Fourier Transform analysis. Subsequently, the SSH signal was reconstructed for the exact timestamps of the LTER sampling using the *t_tide* package (Pawlowicz et al., 2002). This allowed us to estimate the tidal elevation and phase (through the SSH and SSH gradients) at the time of sampling, which were then included as input features in the statistical and neural network (NN) analyses. Their relationship is illustrated and discussed in Supplementary Material, Figs. S3–S4.

Table 1. The physical and hydrochemical parameters used in the study (short name, units, frequency, and source)

| Data	Unit	Frequency	Source
SPM	mg/L	twice weekly	Sylt Roads Marine Observatory
Chl-a	µg/L	twice weekly	Sylt Roads Marine Observatory
Wind speed and direction	m/s, degrees	hourly mean	Deutscher Wetterdienst
Light	hours	daily	Deutscher Wetterdienst
SSH	m	every 5 minutes	Model reconstruction using 13 harmonics and 2 over-harmonics from TPXO9 and verified with the tidal gauges

2.4 Neural Network

To assess the relative contribution of biotic conditions to SPM concentrations, we employed a forward NN to predict SPM based on environmental input parameters. The approach relies primarily on long-term observational data, thereby enhancing the robustness of the results, complemented by model-derived SSH and its temporal gradient data. Although numerical simulations are also powerful tools in this context, any discrepancies they produce can largely be attributed to the choice of numerical methods and the associated uncertainties, including unresolved processes, boundary conditions, and the spatial and temporal resolution of both modelled and observed data (Skogen et al, 2021). While it does not provide process-based understanding, the NN approach is particularly well-suited for this task, as it offers a cost-efficient and data-driven means to capture complex, non-linear relationships between influencing factors. We conducted several sensitivity experiments (not shown), varying both the

250 network depth and the number of neurons per layer. For the current application, increasing the network
251 depth further did not improve performance.
252 For the first part of the experiment, the primary regression task involved predicting SPM concentrations
253 during the winter season, which is characterized by low biological activity, as indicated by minimal
254 Chl-a concentrations. Focusing on winter allows for a clearer assessment of physical (abiotic) drivers,
255 such as wind forcing, with reduced biological confounding. The input features, 19 in total, of the NN
256 model include wind magnitude at the time of sampling and averages over a series of prior time intervals
257 (6 to 240 hours, corresponding to the intervals analyzed in Subsection 3.2.2), dominant wind direction
258 over 6 and 12 hours (even though the correlation analysis shows only a minor impact, the non-linear
259 effects of wind direction may still be present), salinity, SSH, and the temporal gradient of SSH
260 (computed using a forward scheme). The results of the winter model are presented in Section 3.3.1.
261 To extend the analysis across seasons, we applied the same model architecture to the full dataset,
262 initially using the same input features as in the winter setup (results in Section 3.3.3), and subsequently
263 incorporating two additional features: temperature and the weekly sum of sunshine hours before the
264 measurement date (21 features in total, Section 3.3.4). The latter serve as a pragmatic proxy for both
265 Chl-a concentration and benthic algae abundance. While we do not attempt to separate these
266 mechanisms individually, this approach is exploratory and intended to approximate their combined
267 influence on seasonal SPM variability.
268 The technical details of the NN architecture are provided in the Supplementary Material, together with
269 the complete predictor list in Table S2.

3 Results

271 Figure 2 presents the time series of SPM concentrations at the deep and shallow stations in the Sylt-
272 Rømø Bight from 2000 to 2019, based on data from the Sylt Roads monitoring program (Section 2.3.1;
273 station locations shown in Fig. 1). Both stations display a pronounced seasonal cycle, with SPM
274 concentrations typically peaking in winter and declining during summer. The deep station shows more
275 frequent and sustained seasonal peaks in SPM concentrations throughout the time series, whereas the
276 shallow station tends to exhibit higher concentrations during peak events. It is also important to note
277 that the regular sampling at the shallow station was discontinued after 2013 following the replacement
278 of the research vessel, resulting in reduced data coverage in subsequent years.
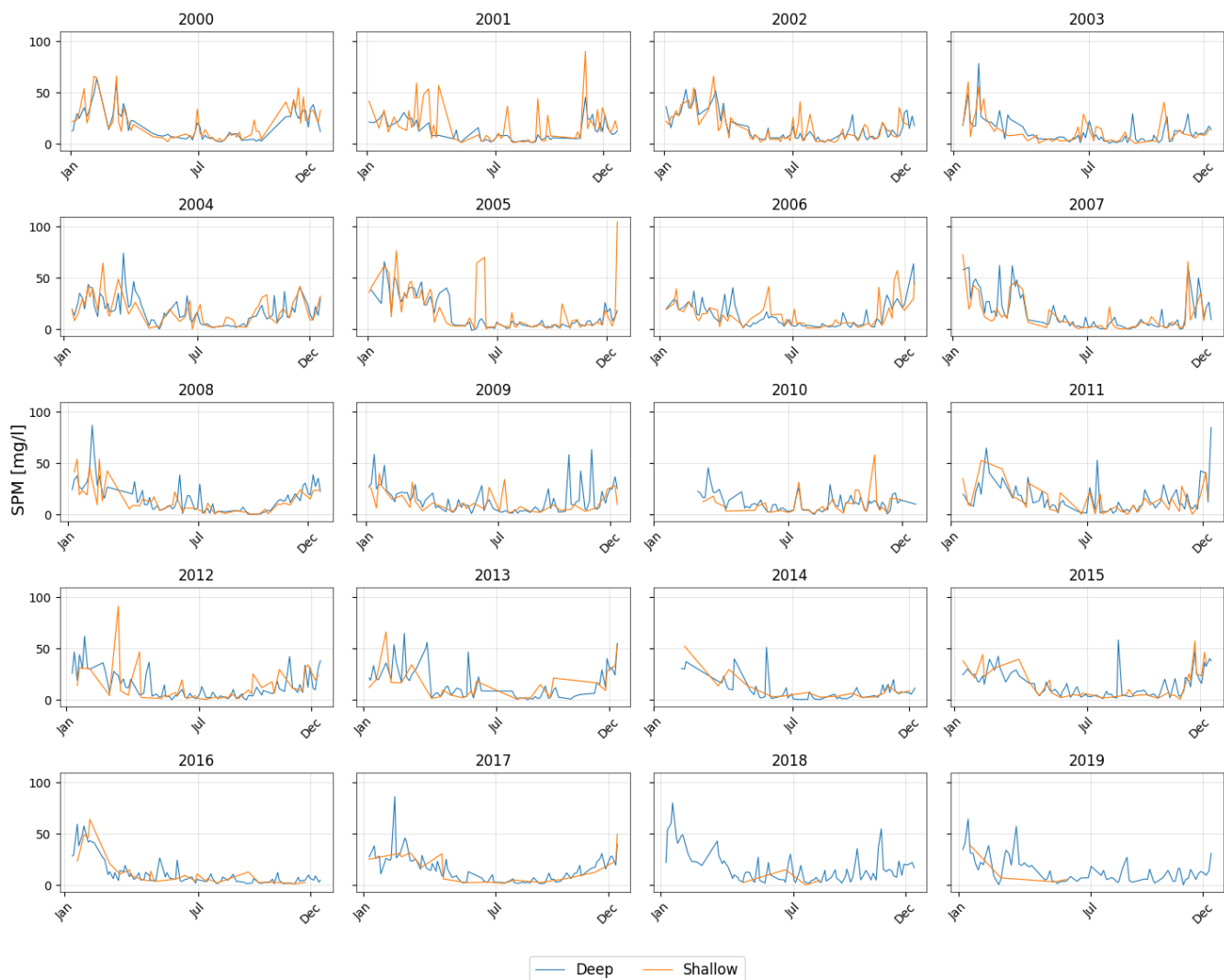
Figure 2: Time series of SPM for the considered years (2000–2019) for the deep (blue) and shallow stations (orange) gridded per year. Each subplot represents a calendar year with time on the x-axis and SPM concentration [mg/l] on the y-axis.

3.1 Seasonality of SPM concentrations

SPM concentrations show an apparent seasonality, which is further investigated in relation to biological activity and meteorological drivers in the subsequent analyses. Using Chl-a as a proxy for phytoplankton biomass, this subsection applies statistical analysis to examine how biological activity and wind forcing together shape seasonal patterns of SPM variability at both the deep and shallow stations.

3.1.1 Role of biological processes in seasonal SPM variations

Both stations exhibit distinct seasonal variations in SPM and Chl-a concentrations (Fig. 3). SPM concentrations are highest in late autumn and winter, with median values of about ~28 mg/L (33.9 ± 18.2 mg/L) at the deep and median of ~26 mg/L (38.6 ± 16.4 mg/L) at the shallow stations. In January, the peak reaches over 60 mg/L at both stations, with individual events exceeding 70 mg/L. The decline in concentrations is observed from February to May, reaching their lowest values in June to August (around 2-3 mg/L), although occasional peaks above 30-40 mg/L still occur. From September onward, SPM begins to increase. This pattern is similar at both stations, though the shallow station generally has slightly higher SPM concentrations, suggesting potential differences in sediment availability or resuspension dynamics.

Chlorophyll-a concentrations follow an inverse seasonal pattern. It remains low in December–January with a median around 2 µg/L (2.1 ± 0.7 µg/L) at both stations. It increases sharply in early spring, with peaks in March-April exceeding 30 µg/L at the deep station and 25 µg/L at the shallow station. Concentrations then drop in summer, followed by a secondary increase in August–October, when values up to ~15-20 µg/L are observed.
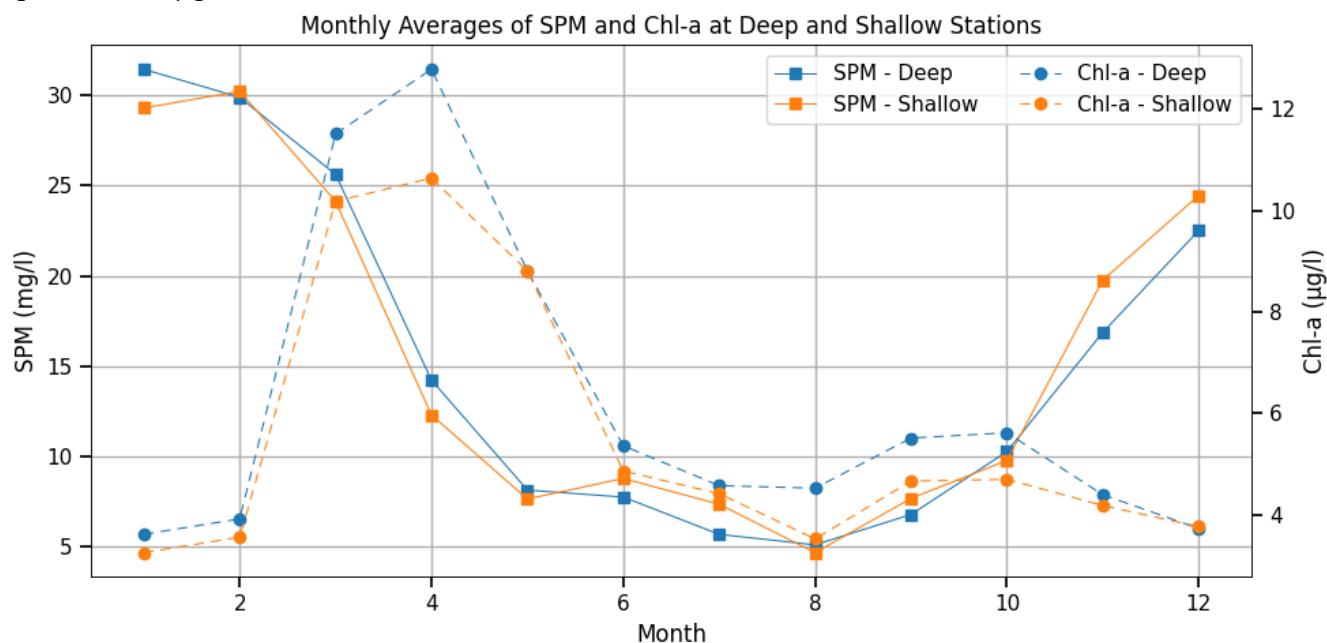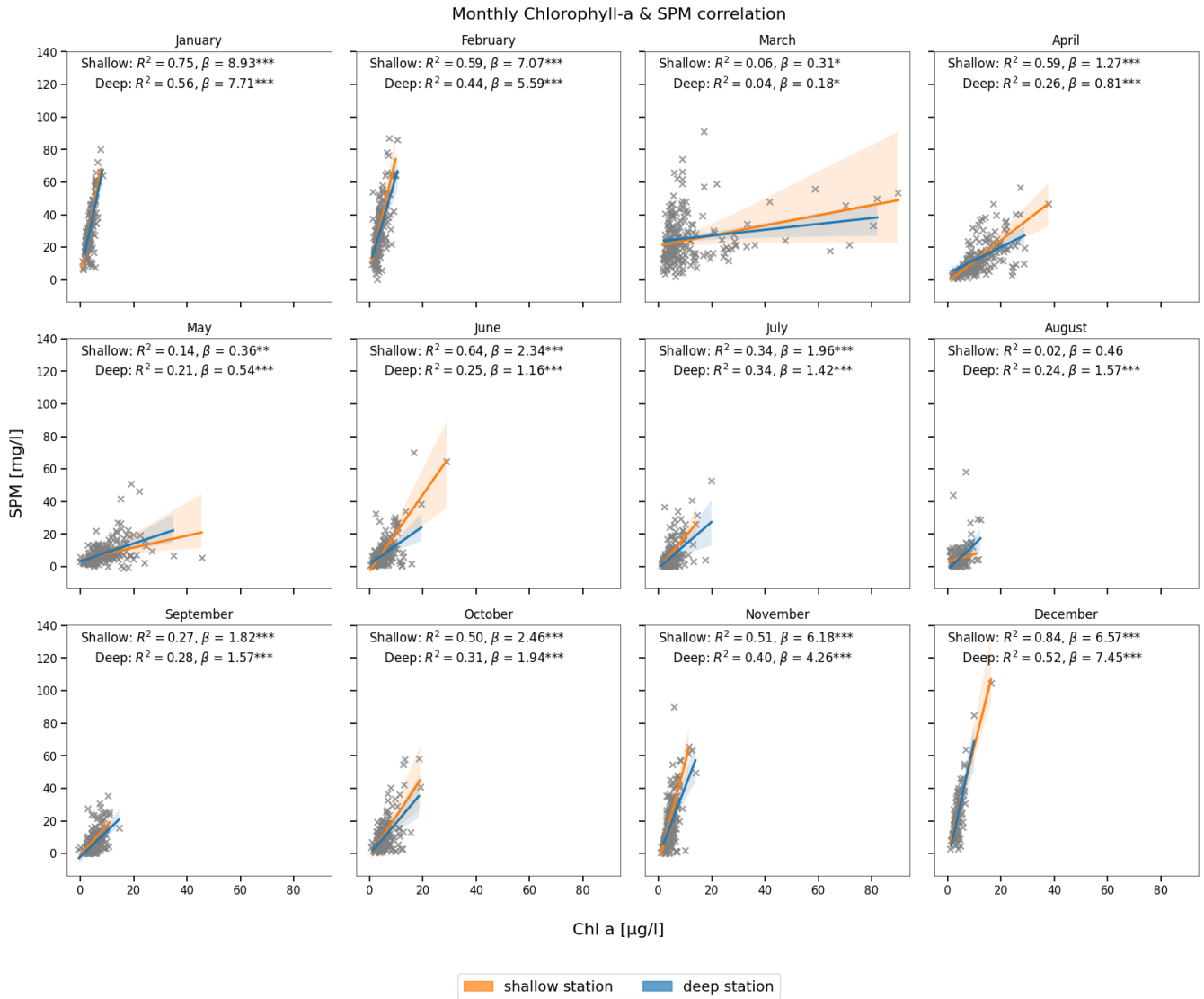

Figure 3: Monthly averages of SPM and Chl-a at the deep (blue) and shallow (orange) stations for the considered years (2000–2019). SPM concentrations solid line with square marker, left axis) and Chl-a concentrations (dashed line with circle markers, right axis) are displayed separately for clarity. The x-axis represents the months from January to December.

The relationship between Chl-a and SPM varies across seasons (Fig. 4). During December–February, biological activity is low and Chl-a constitutes a relatively constant fraction of total SPM, both subject to the same resuspension-deposition processes. This co-settling behavior leads to strong positive correlations observed at both stations. The highest values occur at the shallow station, with $R^2 = 0.84$ in December and $R^2 = 0.75$ in January. At the deep station, correlations are relatively lower, reaching $R^2 =$

11

312   0.52 in December and $R^2 = 0.56$ in January. The strong correlation and the slope are in line with the
313   resuspension of microphytobenthos as observed in winter by de Jonge and van Beusekom (1995). From
314   March onward, the relationship becomes more complex. As Chl-a rises rapidly during the spring bloom
315   and SPM concentrations decline, the correlation at both stations weakens with R^2 values dropping to
316   near-zero in March. This divergence reflects differences in vertical distribution and settling behavior.
317   While phytoplankton is a component of SPM and both are retained on the filter, their decoupling in
318   spring and summer may reflect that not all phytoplankton is floc-associated. Active phytoplankton may
319   remain suspended near the surface, while denser biomineral flocs sink more rapidly, leading to weaker
320   correlations in integrated surface samples. This non-linear and temporally variable influence of Chl-a
321   also underlies the decision not to use it directly as a predictor in the neural network (Section 3.3), but
322   instead to approximate biological activity through more general proxy variables such as temperature and
323   light availbility (see Table S2 in Supplementary Material). During June–August, as both the SPM and
324   Chl-a concentrations reach low values, the correlation weakens further, with August showing almost no
325   correlation at the shallow station. In November and December the correlation strengthens again as the
326   role of biological activity reduces and physical drivers become dominant again.

Monthly Chlorophyll-a & SPM correlation

Panel	Shallow	Deep
January	$R^2 = 0.75, \beta = 8.93$***	$R^2 = 0.56, \beta = 7.71$***
February	$R^2 = 0.59, \beta = 7.07$***	$R^2 = 0.44, \beta = 5.59$***
March	$R^2 = 0.06, \beta = 0.31$*	$R^2 = 0.04, \beta = 0.18$*
April	$R^2 = 0.59, \beta = 1.27$***	$R^2 = 0.26, \beta = 0.81$***
May	$R^2 = 0.14, \beta = 0.36$**	$R^2 = 0.21, \beta = 0.54$***
June	$R^2 = 0.64, \beta = 2.34$***	$R^2 = 0.25, \beta = 1.16$***
July	$R^2 = 0.34, \beta = 1.96$***	$R^2 = 0.34, \beta = 1.42$***
August	$R^2 = 0.02, \beta = 0.46$	$R^2 = 0.24, \beta = 1.57$***
September	$R^2 = 0.27, \beta = 1.82$***	$R^2 = 0.28, \beta = 1.57$***
October	$R^2 = 0.50, \beta = 2.46$***	$R^2 = 0.31, \beta = 1.94$***
November	$R^2 = 0.51, \beta = 6.18$***	$R^2 = 0.40, \beta = 4.26$***
December	$R^2 = 0.84, \beta = 6.57$***	$R^2 = 0.52, \beta = 7.45$***

Figure 4: Monthly correlation between Chl-a (x-axis) and SPM (y-axis) concentrations at the deep (blue) and shallow (orange) stations. The coefficient of determination (R^2), slope (β), and statistical significance (*$p < 0.001$, **$p < 0.01$, *$p < 0.05$) are indicated in each panel.**

3.1.2 Role of wind forcing in seasonal SPM variations

The relationship between seasonal SPM concentrations and wind characteristics is illustrated in Fig. 5. Wind speeds are highest in January, averaging around 8.5 ± 2.8 m/s, with peaks reaching 14.2 ± 1.7 m/s, and gradually decline through spring months, reaching a minimum with mean speeds around 6.5 ± 3.1 m/s and minima of 2.0 ± 0.7 m/s in July–August. From August onward, wind speeds begin to rise again. This seasonal cycle aligns with the observed variability in SPM, with higher concentrations in winter and lower values in summer. Dominant wind directions also vary throughout the year, with

13

westerly and northwesterly winds prevailing in most months, easterly winds in April, and more southerly winds during October–November. Seasonal wind roses illustrating these patterns are shown in the Supplementary Material (Fig. S1). However, no clear linear relationship emerges between dominant wind direction and seasonal SPM concentrations. To account for potential non-linear interactions that may still play a role, wind direction was included as an input feature in the NN model.
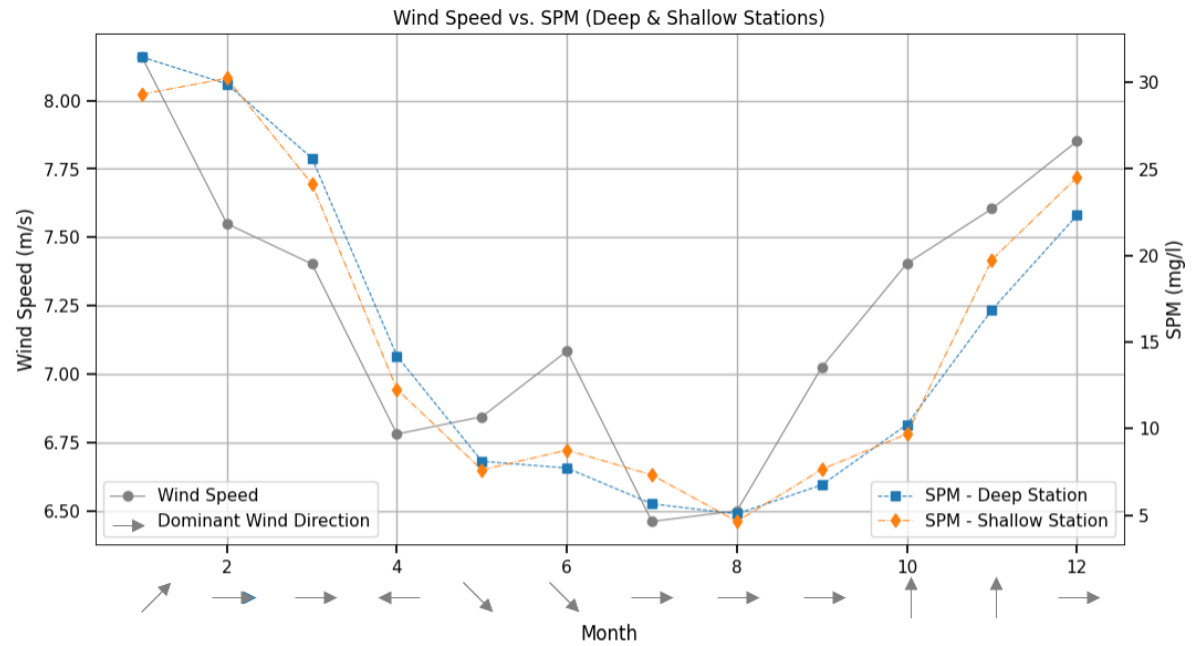
Figure 5: Monthly averages of wind speed, SPM concentrations, and dominant wind direction (2000–2019). The figure illustrates monthly mean wind speed (grey solid line, left axis) and SPM concentrations at the deep (blue squares) and shallow (orange diamonds) stations (right axis). Grey arrows along the x-axis represent the dominant wind direction for each month, with arrow orientation indicating the direction from which the wind originates, following standard meteorological convention.

While correlations are further explored in Section 3.2, the seasonal alignment of wind intensity and SPM concentrations suggests strong physical modulation.

3.2 Resuspension and Time Scales of Inner Basin Transport

Beyond seasonal variation, there are mechanisms responsible for the variability of SPM concentrations on shorter temporal scales, from hours to days. This subsection examines how wind-induced resuspension operates over different time frames and the role of tidal transport within the basin.

### 3.2.1 Role of wind forcing in short time SPM variations

To quantify the short-term response of SPM to wind forcing, we computed Pearson correlation coefficients between SPM concentrations and wind speed averaged over different time intervals, ranging from 1 hour to 240 hours. This approach, commonly referred to as "wind memory," allows us to evaluate how the cumulative influence of past wind conditions affects SPM variability at different depths and over varying time scales. Figure 6 illustrates how the strength of this relationship evolves as

14

wind speeds are averaged over progressively longer intervals, ranging from 1 hour to 240 hours. This approach quantifies how SPM responds to the cumulative influence of past wind conditions over varying time scales. The results show that correlation coefficients generally increase as wind memory lengthens, reaching a peak around 12-18 hours at the shallow station and 120 hours at the deep station, followed by a slight decline.

Monthly variations in the correlation patterns are provided in the Supplementary Material (Fig. S2), showing that the correlation between wind speed and SPM is generally stronger in winter than in summer, with more complex patterns during transitional months such as April and November.
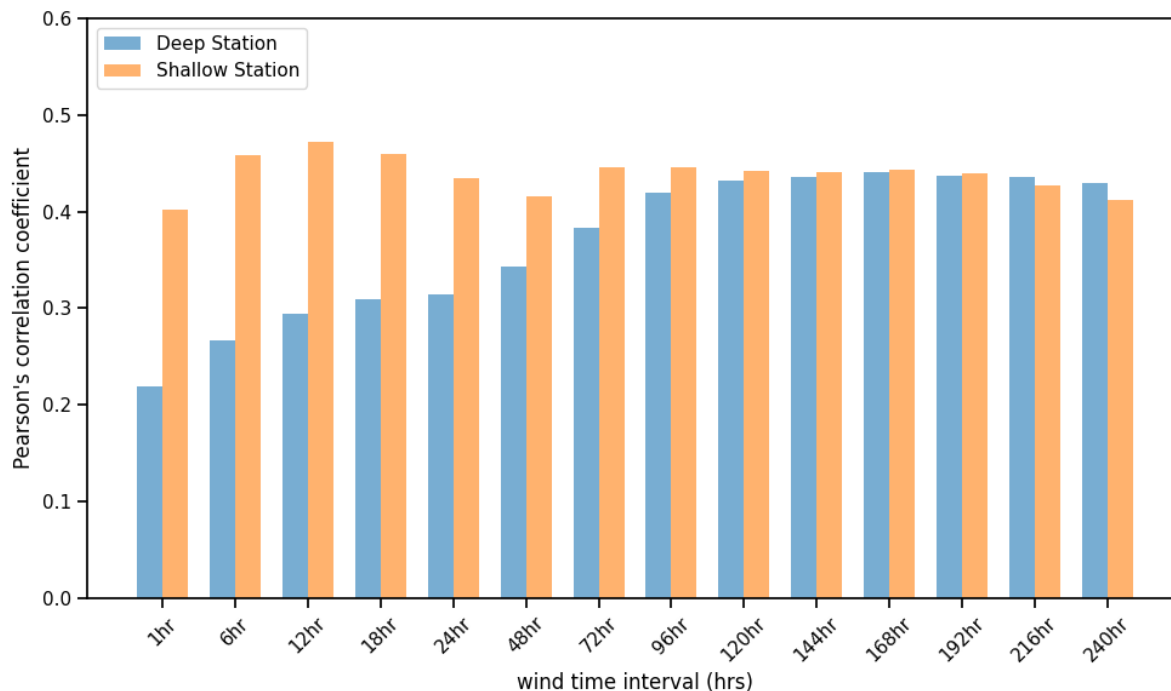
Figure 6: Pearson correlation coefficients between SPM and wind speed averaged over different time intervals, ranging from 1 hour to 240 hours. The two stations (deep station as blue and shallow station as orange) are represented separately, showing how wind memory influences SPM variability at different depths.

The correlation between instantaneous wind speed and SPM concentrations is strongest during winter and early spring (Fig. 7), particularly at the shallow station, where the most substantial value occurs in January ($R^2 = 0.44$) and April ($R^2 = 0.50$). In contrast, the deep station shows much weaker correlations, with R^2 values often near zero, reflecting a lagged effect on SPM concentrations.

During June–August, the relationship weakens significantly, with the lowest correlations observed in August for both stations. The shallow station maintains minor correlation ($R^2 \approx 0.15$) into late summer and early autumn.
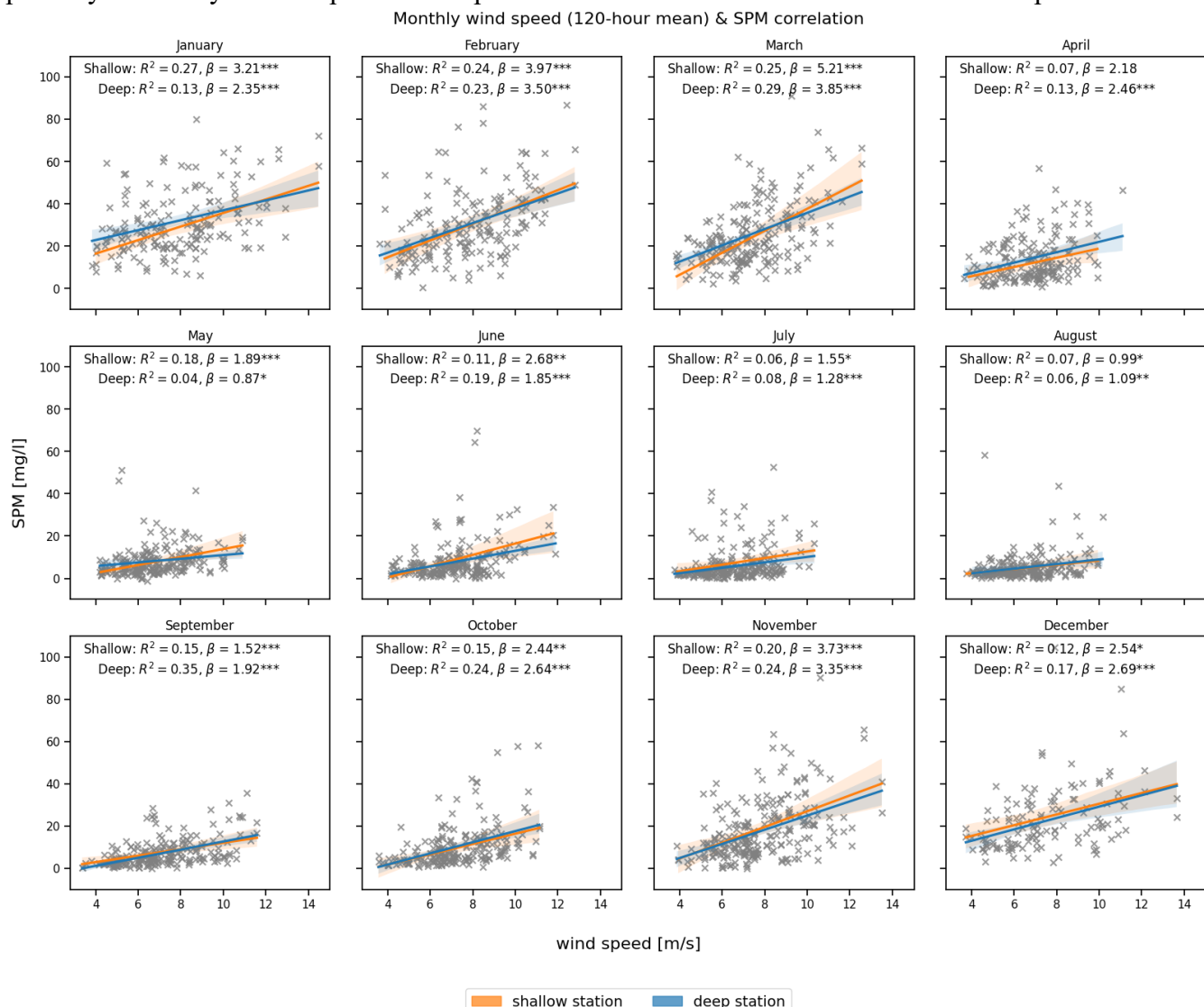
Monthly wind speed & SPM correlation
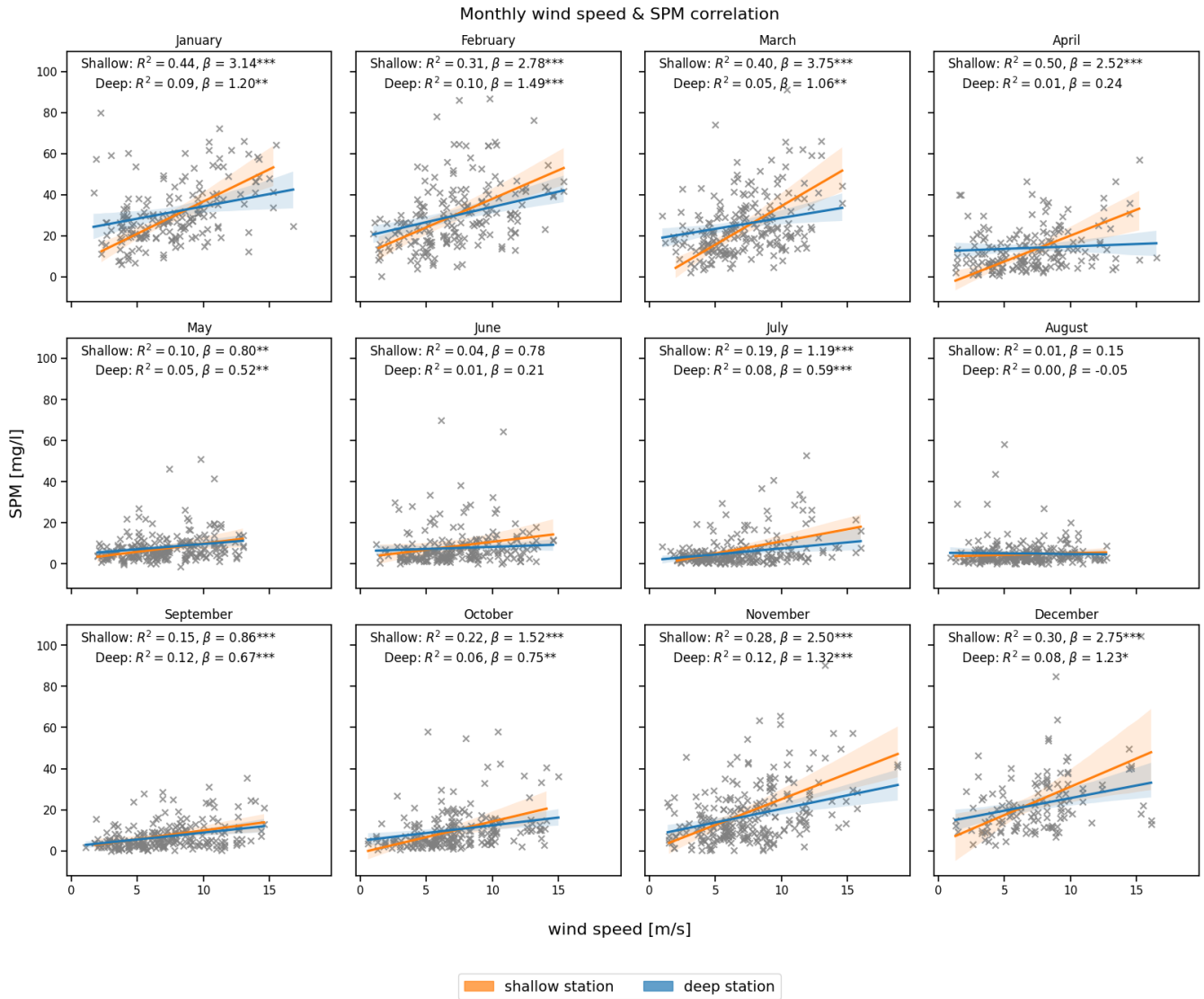
Figure 7: Monthly correlation between wind speed at the time of sampling (x-axis) and SPM concentration (y-axis) at the deep (blue) and shallow (orange) stations. The coefficient of determination (R^2), slope (β), and statistical significance (*p < 0.001, **p < 0.01, *p < 0.05) are indicated in each panel.**

In contrast to the instantaneous impact of wind-speed, averaging wind speed over 120 hours (5 days) results in an improved correlation between wind and SPM at the deep station, as shown in Fig. 8, although the seasonal pattern remains similar. The stronger relationship is particularly evident in the winter and autumn months, especially at the deep station (e.g., R^2 = 0.35 in September, 0.24 in November and February). These findings indicate that the average wind-speed over several days have a stronger influence on SPM concentrations at the deep station than the wind at the time of sampling. The results highlight the role of wind forcing in modulating SPM concentration variability, particularly in shallow waters during winter and autumn. Naturally, the influence of wind is less pronounced in

16

deeper waters through direct resuspension mechanisms. However, it remains significant, with a time lag possibly caused by the transport of resuspended material from shallower zones to the deep station.


Figure 8: Monthly correlation between wind speed averaged over a 120-hour (5-day) period (x-axis) and SPM concentration (y-axis) at the deep (blue) and shallow (orange) stations. The coefficient of determination (R²), slope (β), and statistical significance (***p < 0.001, **p < 0.01, *p < 0.05) are indicated in each panel.

3.2.2 Role of tidal forcing in short time SPM variations
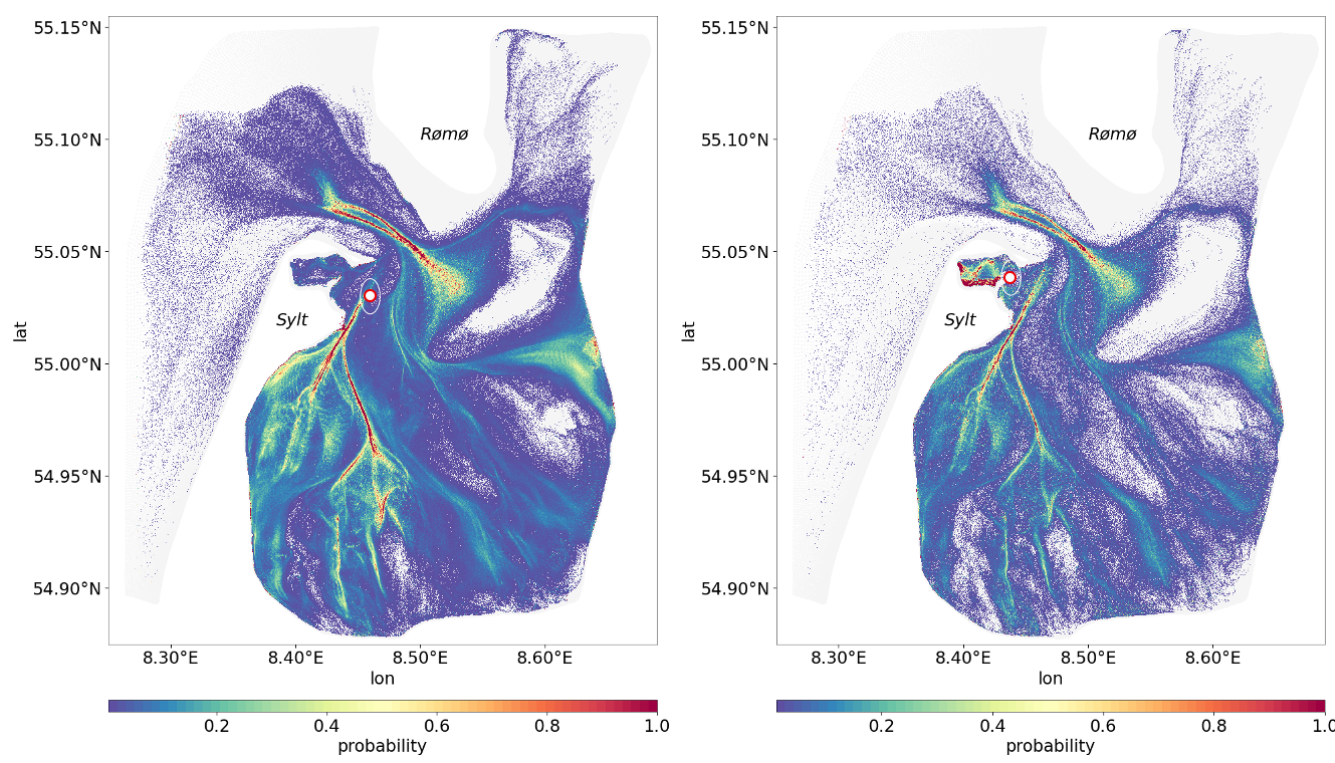
Figure 9: Probability distribution of passive tracer pathways to illustrate how frequently different areas act as source regions or transport corridors for passive tracers. Higher probability values (highlighted in yellow and red) indicate locations that more frequently contribute to SPM reaching the deep station (left panel) or shallow station (right panel).

Figure 9 shows the spatial probability distribution of passive tracer connectivity within the basin, derived from Lagrangian simulations forced solely by tides. This setup isolates the dominant physical driver of material transport in the Sylt-Rømø Bight, where tidal processes account for roughly 80% of velocity variability (Fofonova et al., 2019). While regular wind forcing (excluding storm events and uncommon multi-day episodes of strong winds from a single direction) enhances lateral dispersion, its net contribution to basin-wide transport over several days is relatively minor (Konyssova et al., 2025). Note, in this region, typical wind events last about 5–6 hours, defined as consecutive hours of wind from the same direction within an eight-sector classification (Rubinetti et al., 2023). Residual currents generated by non-linear tidal interactions establish consistent, directional transport pathways, which are effectively captured by the simulated tracer trajectories.

The resulting network of tidally-induced transport pathways reveals apparent differences between the two stations. The shallow station is predominantly supplied by tracers originating in the northern parts of the bight, particularly Königshafen and its surroundings, reflecting localized and relatively rapid connections. In contrast, the deep station is influenced by broader and more distributed transport pathways, integrating material from a wider area of the basin.

18
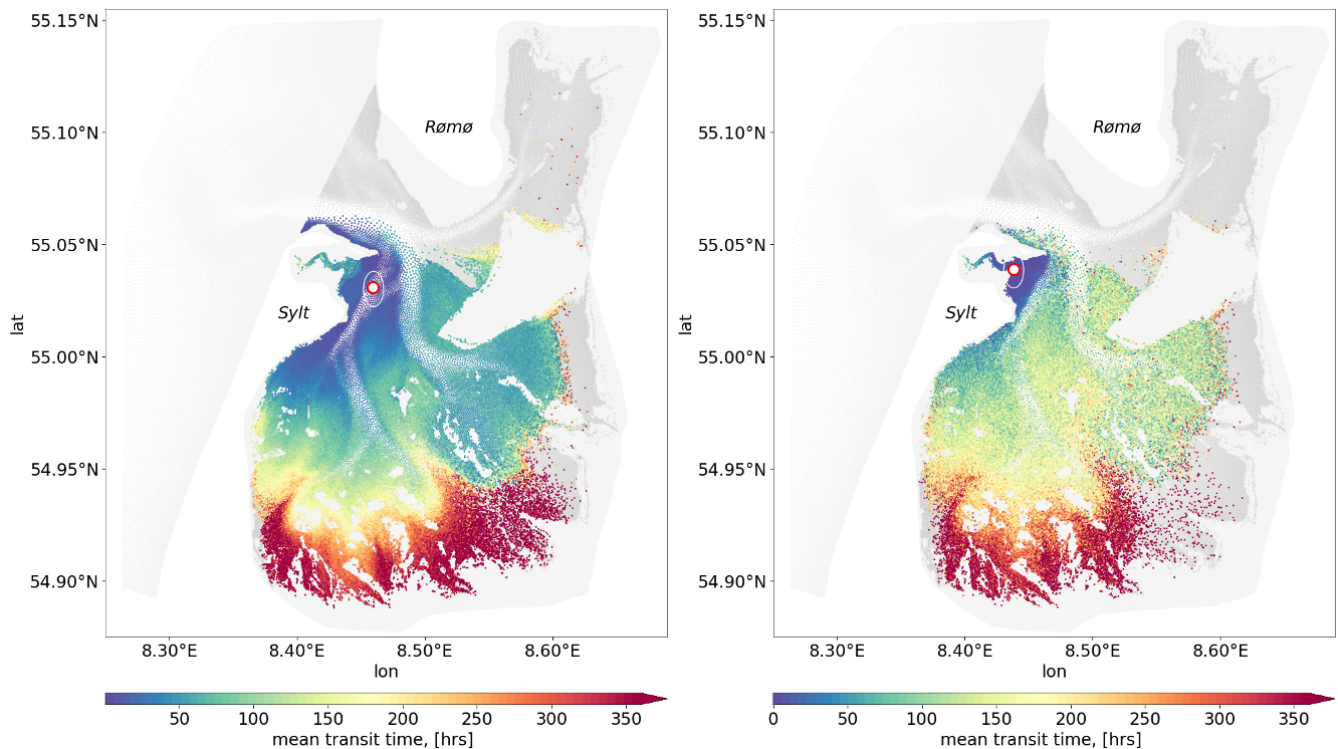
Figure 10: The mean transit time of passive tracers to reach the sampling station. The left panel corresponds to the deep station, while the right panel represents the shallow station. Grid elements that are consistently inundated with each flood phase, from which the passive tracers are released, are shown in grey. Elements that successfully reach one of the two sampling stations are colour-coded by their mean transit time (in hours), reflecting how long it takes for passive tracers to reach from a given location to each station.

For both stations, shorter transit times (depicted in blue and green, Fig. 10) are observed in areas closer to the stations, whereas regions further away, particularly in the inner tidal flats, exhibit longer transit times (yellow to red hues, Fig. 10). The transit time patterns reveal that SPM originating from intertidal areas and tidal channels follows particular pathways before reaching the deeper and shallower monitoring stations, with transport occurring on timescales of days to weeks. The difference between the two panels suggests that the deep and shallow stations receive material from primarily distinct but partially overlapping source regions.

Together, these figures illustrate the tidal connectivity of the two monitoring stations with their surrounding basin, highlighting likely source regions and typical transport pathways. To quantify the typical timescale for SPM transport, a probability-weighted transit time was computed, where individual transit times were weighted according to their interpolated probability values. This approach ensures that the estimated transit time reflects the most frequently occurring transport pathways rather than rare, low-probability trajectories. The resulting probability-weighted median transit time was 133.3 hours for the deep station, which aligns with the ~5-day wind-memory interval identified in Section 3.2.2, and 44.4 hours for the shallow station, highlighting the pronounced contrast in transport efficiency between the two locations and likely reflecting differences in sediment source regions. Although not explicitly resolved in the simulations, this difference may also relate to grain-size

19

440 composition, as the deeper channels typically contain coarser material, whereas the intertidal flats have
441 finer, more cohesive sediments (Bartholomä et al., 2009). At the shallow station, which is situated
442 within the Königshafen area, SPM concentrations respond to wind forcing almost immediately through
443 local resuspension. The longer transit time therefore does not indicate a delayed response, but rather
444 reflects the additional supply of tracers arriving from a wider surrounding area, which extends the
445 median transit time beyond the short wind-driven response captured in the memory analysis. In contrast,
446 the deep station integrates SPM from more complex, multi-step transport routes over longer timescales.
447 These transit times provide a key reference for interpreting observed SPM fluctuations at each station
448 and may help distinguish between short-term and cumulative drivers of SPM variability.

449 **3.3 Neural Network**

450 **3.3.1 Winter SPM prediction (Baseline Model)**
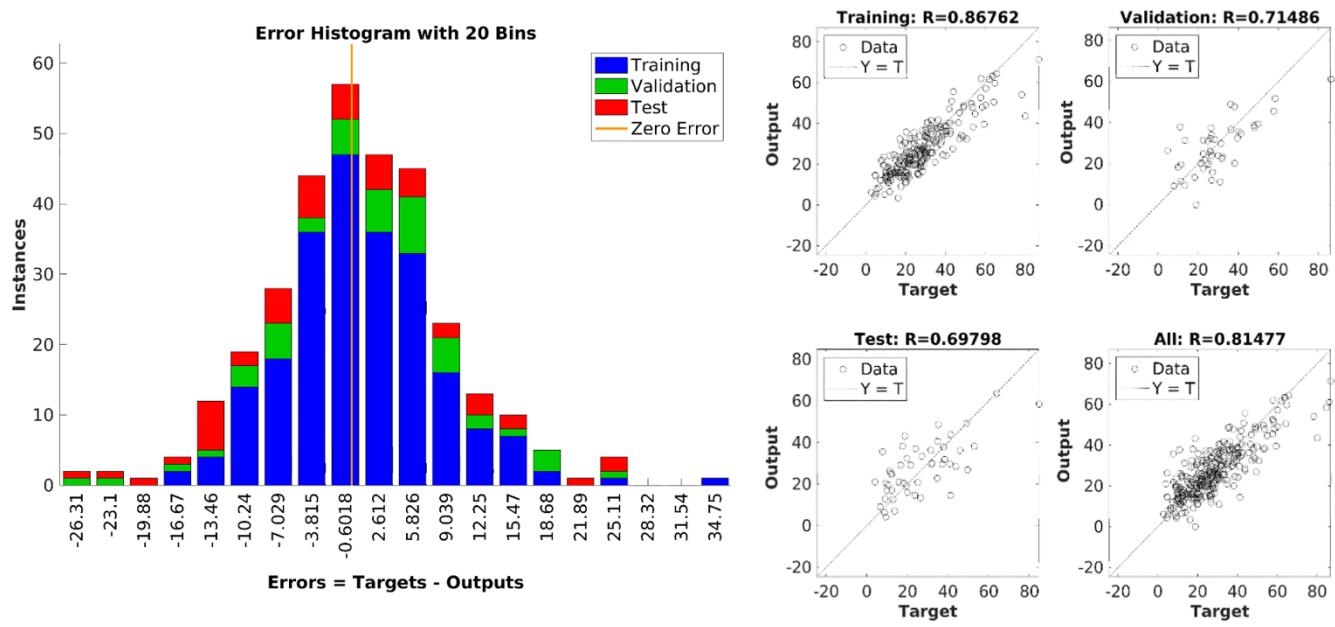
451
452 **Figure 11: Performance of the neural network (NN) trained on the winter dataset for the deep station. Left: Error histogram**
453 **showing the distribution of prediction errors (in mg/L) for training, validation, and test subsets. Right: Regression plots**
454 **comparing predicted vs. observed SPM values, with correlation coefficients (R) for each data subset. Due to the overall qualitative**
455 **similarity between the pictures for deep and shallow stations, only the deep station is presented here.**

456 To evaluate how well physical drivers alone can explain SPM concentration variability, we first trained
457 a baseline NN using only the winter dataset, when biological activity is minimal. This provides a
458 reference to assess the contribution of wind and tidal forcing under conditions with limited biological
459 influence.
460 The error for training, validation and testing has a normal distribution (Fig. 11, left). For the deep
461 station, the root mean square error (RMSE), a measure of average prediction error magnitude, is 9.4
462 mg/L for the testing set. Note that the observed mean and median SPM concentrations in winter are 27.6

20

and 25.9 mg/L respectively. As a result of the application of NN to the winter dataset, they are 27.2 and 25.5 mg/L respectively (Table 2). Regression analysis (Fig. 11, right) yields correlation coefficients between observed and simulated SPMs equal to ~0.87, ~0.71, ~0.7 and ~0.81 for training, validation, testing and all winter datasets, respectively.

The results show that, by using tidal and wind forcing along with a proxy for baroclinic conditions (salinity), we can predict SPM concentrations during winter quite well without accounting for other factors.

Notably, temperature, salinity, turbulent kinetic energy, and SPM concentrations themselves all influence flocculation processes, even without considering biological activity. Temperature was excluded from the feature set at this stage due to its strong seasonal cycle and its potential use as a proxy for biological conditions. Specifically, in our current approach, we cannot separate the influence of temperature on biological mechanisms from its physical effects (e.g. viscosity), which also impact flocculation.

### 3.3.2 Applying of NN trained on winter data to other seasons

Next, we applied the NN trained under winter conditions to other seasons. This approach is justified by the fact that the long-term dataset captures a representative range of wind conditions in both winter and summer, including calm periods and strong wind events. Furthermore, salinity remains relatively stable across seasons, supporting the applicability of the model. Using the trained winter model, we attempt to predict SPM concentrations for spring, summer, and autumn. The goal of this step is to estimate the influence of biological processes on SPM concentrations.

For both stations, the results of the NN application show significantly higher SPM concentrations compared to observations (Table 2).

Table 2. Mean, median values and correlation (R) of SPM concentrations, [mg/L], from observations VS predictions by NN trained on winter dataset for the deep and shallow stations

seasons		Deep Station		Shallow Station	
		observed	predicted	observed	predicted
winter	mean, [mg/L]	27.6	27.2	28.5	24.7
	median, [mg/L]	25.9	25.5	24.4	26.5
		R = 0.81		R = 0.81	
spring	mean, [mg/L]	16.5	24.8	15.6	20.6
	median, [mg/L]	13.3	24.3	11.3	18.0
		R = 0.29		R = 0.5	
summer	mean, [mg/L]	6.15	17.7	6.8	18.5
	median, [mg/L]	4.22	16.9	3.9	16.1
		R = 0.04		R = 0.35	

autumn	mean, [mg/L]	11.6	23.4	12.8	24.0
	median, [mg/L]	8.5	22.7	7.5	21.0
		R = 0.44		*R = 0.54*	
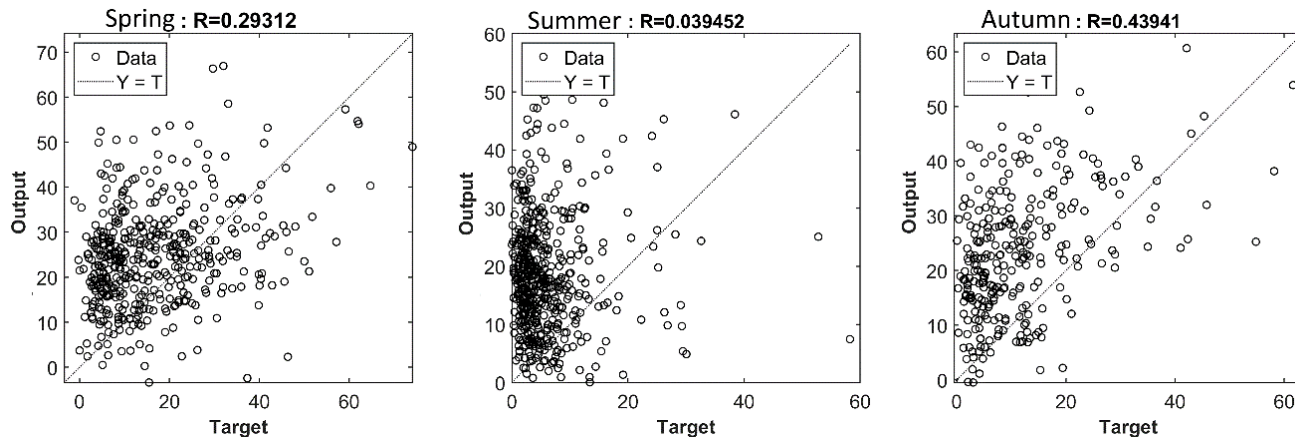
Figure 12: Regression analysis for NN trained on winter data and applied to spring, summer and autumn data vs observations. Results shown for the deep station; shallow station results are qualitatively similar and summarized in Table 2.

This discrepancy suggests that while calmer wind conditions alone can explain approximately 40% of the SPM reduction in summer compared to winter, they do not account for the full ~80% decrease observed in the data (see Table 2). The overestimation of SPM by the NN is clearly visible in the regression plots (Fig. 12), where most of the predicted values are positioned above the Y = T line, particularly during summer and autumn. This does not necessarily imply that biological activity is weaker in spring, but rather that its impact is less well captured by the abiotic-only model, as biological processes contribute more strongly to variability than in autumn. The higher correlation between simulated and observed SPM in autumn likely reflects physical conditions that are more similar to winter, when the model was trained, including generally stronger winds (Section 3.2.2). In spring, enhanced biological activity and aggregation introduce variability that the model cannot account for, reducing correlation. During summer, the regression coefficient dropping below 0.05 indicates that processes not represented in the abiotic model become dominant (Fig. 12). The subsequent analysis of all seasons presented in Section 3.3.3 points to biologically mediated mechanisms, such as flocculation and sediment stabilization, as the main contributors to this variability.

3.3.3 NN trained at the data from all seasons

Previously we showed that there are factors, in particular biological processes, which significantly influence the SPM dynamics. To confirm this, we trained NN on all the dataset (not limited to winter) using the same input features representing only abiotic conditions, which we used in 3.3.1. As expected, the overall RMSE increases to approximately 11 mg/L, due to the omission of important features that influence SPM dynamics during the warm season (Supplementary Fig. S5). When the model is trained on data from all seasons, and applied specifically to winter conditions, it

22

underestimates SPM concentrations. For the deep station, the predicted mean and median are 19.17 mg/L and 17.2 mg/L, respectively, compared to observed values of 27.6 mg/L and 25.9 mg/L. At the shallow station, the model yields mean and median predictions of 20 mg/L and 17 mg/L, whereas the corresponding observed values are 28.45 mg/L and 24.35 mg/L. The regression coefficients also reflect this underperformance, with values of approximately $R \approx 0.66$ (deep) and 0.72 (shallow). The seasonal regression analysis further highlights these biases (Supplementary Fig. S7, upper row). A complete numerical breakdown of observed and predicted seasonal values is provided in Table S3.

3.3.4 Neural network trained on all-season data including biological proxy features

Including temperature and sunshine duration as proxies for biological activity improved overall model skill, reducing the test RMSE to ~10 mg/L. The regression analysis shows the correlation coefficient between observed and simulated SPM concentrations reached ~0.88, ~0.76, ~0.72 and ~0.84 for training, validation, testing and all datasets respectively (Supplementary Fig. S6). Seasonal regression plots also show marked improvements (Supplementary Fig. S7, lower row). For winter, R increased from 0.66 to 0.73 at the deep station and from 0.72 to 0.82 at the shallow station. The largest gains occurred in spring and summer, consistent with more substantial biological influence during these seasons. Table S3 provides the detailed seasonal comparison of observed and predicted means, medians, and correlations.

4 Discussion

This study set out to investigate the combined influence of wind forcing, tidal transport, and biological processes on SPM concentration variability in the Sylt-Rømø Bight. Using 20-year period monitoring data and applying statistical tools, neural network models, and Lagrangian simulations, we analyze the relative roles of these processes across seasonal and short-term timescales.
The variability observed in SPM concentrations reflects the inherent complexity of the system, where several physical and biological mechanisms interact across different spatial and temporal scales. Wind-driven resuspension, tidal advection, and biologically mediated effects each contribute to the observed dynamics, with their relative importance shifting seasonally. This complexity highlights that the variability in SPM concentrations cannot be attributed to a single driver but rather to the combined response of the system to multiple, overlapping processes.
In this chapter, we will further discuss topics that have not yet been fully addressed: the peculiarities of the Chl-a and SPM concentration relationship, biological processes that directly or indirectly influence SPM dynamics, further details on wind and tide control including SSH and SPM concentration relationship, details of NN related findings and study limitations.

4.1 Biological Interaction

The strong positive correlation between Chl-a and SPM concentrations in winter suggests that under low biological activity, such as limited phytoplankton growth, behaviour of both variables is driven mainly by physical processes such as wind-driven resuspension. This is consistent with previous

observations in the Wadden Sea and German Bight (van Beusekom et al., 1999; van Beusekom and de Jonge, 2002). Together with SPM, the strong winds resuspend microphytobenthos attached to sediment particles (de Jonge and van Beuseukom, 1995), consistent with observations by Hommersom et al. (2009), who found strong correlations between SPM and Chl-a in the Wadden Sea driven by resuspension. Such patterns support the interpretation that, under winter conditions with low biological production, a large fraction of Chl-a is contained within resuspended flocs, leading to the high correlations observed in our study at both stations. In contrast, the correlation between Chl-a and SPM concentrations begin to decline in spring, despite persistent wind forcing, and reaches a minimum in summer. This seasonal decoupling suggests that biological aggregation processes become increasingly dominant with the beginning of and following phytoplankton bloom, promoting the formation and subsequent rapid settling of flocs (Schartau et al., 2019; Maerz et al., 2016; Lunau et al., 2006). For example, the production of TEPs, secreted by phytoplankton and bacteria under certain physiological or nutrient conditions, strongly enhance particle stickiness and promote the aggregation of both organic and mineral particles (Passow, 2002). While our statistical analysis (however, not NN related efforts) uses Chl-a as a proxy for biological activity, it is worth noting that TEP production responds to additional drivers such as nutrient status and species composition, which can modulate flocculation potential even at similar Chl-a levels. In addition to the biological feedback, the increase in water temperature during summer also accelerates particle sinking rates by reducing water viscosity, further promoting sediment deposition (Maerz and Wirtz, 2009). This supports the view that the Chl-a–SPM relationship reflects an interplay of multiple biological and physical controls rather than a single, direct pathway.

While both spring and autumn are characterized by peaks in Chl-a concentration, their influence on SPM dynamics appears to differ. In spring, calmer conditions favor particle aggregation and settling, often leading to reduced SPM levels. In autumn, however, the secondary bloom coincides with a seasonal increase in wind speed (Fig. 5), resulting in elevated SPM concentrations despite high biological activity. This suggests that enhanced organic matter availability in autumn may promote flocculation, but stronger resuspension prevents effective settling. These seasonal contrasts highlight that biological influence on SPM is strongly modulated by concurrent physical forcing.

In parallel, benthic microbial processes such as biofilm formation by microphytobenthos enhance sediment stability and reduce its susceptibility to resuspension, thereby modulating the amount of SPM remaining in the water column (Andersen, 2000; Stal, 2010). Beyond microbial stabilization, benthic fauna also influences SPM dynamics through benthic-pelagic coupling. Filter-feeding benthos, such as bivalves, consume suspended particulate organic carbon (POC), effectively removing material from the water column and altering vertical fluxes of organic matter. In the Sylt-Rømø Bight, food web modelling by Baird et al. (2004) estimated that benthic consumers remove approximately 56.7 mgC m^{-2} d^{-1} of suspended POC – potentially a substantial fraction of total SPM, depending on the proportion of organic material within it. Benthic consumption likely constitutes a significant sink for fine, organic-rich particles, particularly in areas with dense benthic communities, as filter feeders remove SPM primarily through ingestion and the production of faecal pellets, which promote deposition of organic-rich material to seabed. Although the proportion of POC within SPM is known to depend on total SPM concentration (Schartau et al., 2019), robust SPM-to-POC conversion factors remain uncertain due to the unknown share of freshly formed organic matter. Although the effects of native species on bentho-

589 pelagic coupling have been relatively well studied in the region (Baird et al., 2007), the role of
590 introduced species remains less clear. For example, the introduction and spread of alien species such as
591 the American razor clam (*Ensis leei*) may further amplify benthic filtration effects. In the Dutch
592 Wadden Sea, they have shown to significantly alter trophic carbon flows, increasing carbon
593 consumption by secondary producers and redirecting energy flows away from higher trophic levels
594 (Jung et al., 2020). Although the abundance of *E. leei* in the Sylt-Rømø Bight has not yet been
595 quantified, its potential influence on observed SPM concentrations provides a basis for further
596 investigation as part of long-term ecological changes in the region.

4.2 Wind & Tide Control

598 The results suggest that the intensity of winds, rather than their dominant directions, exerts a stronger
599 influence on the seasonal cycle of SPM. The seasonal patterns of wind speed, with maximum values in
600 winter and minima in summer, aligns closely with the observed SPM concentrations, suggesting a
601 physically mediated control during high-energy periods. During summer, the weaker relationship
602 between wind speed and SPM concentrations points to the increasing importance of biological
603 contribution. These may include enhanced flocculation and settling of particles, increased filtration by
604 benthic organisms, reduced sediment availability due to biological stabilization, and overall calmer
605 wind conditions. Although tidal forcing itself does not vary seasonally, its influence on SPM
606 concentrations also likely changes throughout the year because the sediment properties and biological
607 activity that determine sediment availability and erodibility vary over time.
608 Notably, correlations between wind speed and SPM are stronger at the shallow station compared to the
609 deep station, as the shallow environments are more susceptible to wind-induced turbulence, including
610 wave action. It should be noted that, since the study addresses observations of SPM concentrations,
611 wind-induced resuspension is considered to include the effects of wave action.
612 In addition, the area around the shallow station is characterized by relatively small depths. Therefore, at
613 the shallow station, the short wind-memory intervals (12–18 hours) yield the strongest correlations.
614 Lagrangian simulations support this interpretation by illustrating that the shallow station, located within
615 the intertidal zone itself, receives SPM directly from resuspension at the site. While these simulations
616 do not represent full sediment dynamics, they effectively illustrate dominant source areas and transport
617 timescales. This relatively short response time aligns with earlier observations in tidal flat systems,
618 where wind effects on SPM are immediate in intertidal zones but take longer to become apparent in
619 deeper areas (de Jonge and van Beusekom, 1995).
620 In contrast, the situation at the deep station is more complex. In addition to the larger distance between
621 the observation point and the sea bottom, sediment characteristics in the channels are predominantly
622 sandy, which typically requires stronger wind energy to be resuspended as opposed to the mud and finer
623 material found in intertidal areas (Bartholomä et al., 2009). The delayed response seen in the wind
624 memory analysis (~120 hours) and the tidally modulated transport pathways from our Lagrangian
625 simulations (median transit time ~133 hours) likely reflects the combined influence of episodic wind-
626 driven resuspension in shallow areas and subsequent advective transport to the deeper station
627 (Friedrichs and Perry, 2001; de Jonge and van Beusekom, 1995). Similar multi-day lags in SPM
628 response have been observed in other estuarine systems where tidally dominated transport pathways act

629 on resuspended sediments originating from more energetic, nearshore zones (see also Winterwerp,
630 2001). Together, these results highlight a clear contrast between the two stations: rapid, localized
631 sediment response in the shallow embayment versus slower, more integrated transport processes at the
632 relatively deep channel.
633 The Lagrangian tracer simulations provide additional spatial context, revealing weak connectivity
634 between the north-eastern and southern sections of the Sylt-Rømø Bight under regular tidal conditions.
635 Passive tracers released in the north-eastern region rarely reach either of the sampling stations. This
636 indicates that the stations, while valuable for long-term monitoring, may not fully capture the spatial
637 variability of SPM dynamics across the entire basin, especially on shorter time scales.
638 Beyond local wind and tidal resuspension and transport within the Sylt-Rømø Bight, tidal phases also
639 influence SPM concentrations. Naturally, higher SPM concentrations are associated with lower water
640 levels under otherwise equal conditions, as the measurements are always taken at the surface (Fig. S3).
641 Due to the large role of non-linear processes in the area there is also an asymmetry between flood and
642 ebb in terms of duration as well as mean and maximum velocities.

4.3 Neural Network findings

644 The NN experiments provide a line of evidence supporting the seasonal shift in dominant SPM drivers
645 independent of the statistical analysis. When trained only on winter data, where biological activity is
646 minimal, the NN successfully captured winter SPM concentrations using solely physical drivers such as
647 wind conditions within different time intervals, salinity, and tidal elevation (through SSH and SSH
648 gradient). At both stations, this winter model performed well ($R \approx 0.81$), confirming that physical
649 processes alone can account for most of the observed variability during this season. This reinforces the
650 view that winter dynamics are dominated by abiotic drivers.
651 However, when the same winter-trained model was applied to other seasons, it consistently
652 overestimated SPM concentrations, especially in summer when biological activity is high and wind
653 speed is generally weaker. For example, at the deep station, the observed mean SPM concentration
654 decreased by ~78%, whereas the model reproduced only a ~36% reduction, meaning that less than half
655 of the observed seasonal decline could be explained by abiotic factors. Similarly, at the shallow station,
656 observed SPM declined by 80%, while the model captured only a ~42% reduction, accounting for just
657 over half of the change. These mismatches underscore the increasing importance of biological drivers
658 during the summer months. Interestingly, although both stations showed similar magnitudes of
659 overestimation, the shallow station retained higher predictive skill ($R \approx 0.35$) than the deep station ($R \approx$
660 0.04) in summer. This difference likely reflects the stronger and more immediate influence of wind
661 forcing at the shallow site, where even in summer, intermittent wind events can rapidly mobilize
662 sediments.
663 The addition of biologically relevant features such as temperature and sunshine duration into the full-
664 year NN model, in Section 3.3.4, significantly improved its performance, especially at the shallow
665 station. While we do not explicitly resolve individual biological pathways, these proxies likely capture
666 their cumulative effects as seen from the improved model fit indicating their aggregate influence is both
667 detectable and substantial. These processes may include phytoplankton-driven aggregation and
668 flocculation, microbial stabilization, and bentho-pelagic interactions such as benthic filtration. Our

26

interpretation remains exploratory rather than conclusive, as targeted biological data would be required
to quantify these mechanisms in detail.

4.4 Study Limitations

Although, in this study, we discuss the main driving mechanisms of SPM concentrations in the Sylt-
Rømø Bight, we also acknowledge that the system is far more complex and has more factors
influencing the fluctuations of SPM concentrations than we investigate here. Moreover, the SPM itself
is a parameter that is composed of various components and sizes in nature, and such a level of detail is
not readily available in the dataset. Incorporating measurements of sediment composition (organic
versus inorganic fractions) and their sizes would add more certainty into the roles of considered
mechanisms modifying SPM concentrations.
Our Lagrangian transport simulations use massless passive tracers, which do not account
for flocculation, deposition, or resuspension processes. Incorporating such processes would require a
different modeling framework and additional data that are not currently available, including detailed
habitat maps and reliable estimates of SPM fluxes from the open boundary. Nonetheless, despite these
simplifications, the model effectively captures key patterns of spatial connectivity pathways and
timescales driven by tidal dynamics.
Another limitation is that changes in the SPM input from the open boundary cannot be quantified. Net
coastward transport from the North Sea likely contributes to seasonal variability, for example, through
enhanced import or retention in spring and summer (Burchard et al., 2008; Postma, 1981), but we lack
data to resolve this numerically.
In addition, more precise SPM predictions would benefit from neural network architectures with
"memory", such as Long Short-Term Memory (LSTM) models, which can account for the delayed
effects of biotic and abiotic conditions over several months. A North Sea-wide approach would be
required to capture these long-term dynamics and boundary-driven influences. Within such a
framework, it would also be appropriate to include additional predictors such as nutrient concentrations
and benthic processes to represent better the complex interactions driving SPM variability.
While this study does not claim to offer a comprehensive representation of all the processes in play, we
believe that our work presents new insights to understand better the baseline mechanisms of SPM
concentration variability within the basin and across multiple timescales.

5 Conclusions

This study investigated the primary drivers of SPM variability in the Sylt-Rømø Bight, a semi enclosed
basin with well-mixed conditions and hydrodynamics dominantly shaped by tides. We combined long-
term monitoring data (SPM, Chl-a, wind conditions, and light availability) with SSH reconstructed from
a validated hydrodynamic model, and applied statistical analyses and neural network modelling. In
addition, Lagrangian transport simulations were used to assess tidal connectivity and transport
timescales. Together, these approaches revealed new insights on SPM concentration variability across
multiple timescales and relative influence of the main driving mechanisms.

Our findings confirm that wind speed is the primary driver of short-term SPM variability, particularly at the shallow station, where SPM concentrations respond almost immediately to wind forcing. This rapid response, especially during winter and autumn, highlights the importance of wind-driven resuspension in shallow waters. In contrast, the deep station exhibits a more delayed response to wind forcing, with peak correlations occurring at longer wind memory intervals (~5 days). This lag reflects the fact that, at greater depths, direct resuspension due to immediate wind forcing plays a reduced role, while the transport of material from neighboring shallower areas becomes increasingly important.

Tidal dynamics primarily regulate the advection processes within the basin, redistributing fine, easily resuspendable material from shallow to the deeper areas. Lagrangian simulations illustrate that SPM at the shallow station originates locally, predominantly from within or around the Königshafen embayment. Meanwhile, at the deep station, SPM is likely supplied from the intertidal and shallow areas by the tidally driven redistribution over a longer timescale (~133 hours), consistent with the observed wind-memory lag (~120 hours). These results highlight the fundamental distinction between localized, wind-driven resuspension and slower, broader-scale, tide-driven transport, both of which shape SPM variability but at different spatial and temporal scales.

On seasonal timescales, however, biological processes exert an increasingly strong control. The onset of the spring phytoplankton bloom coincides with a decline in SPM concentrations, likely due to the enhanced production of TEPs and other extracellular polymers that promote biological aggregation and flocculation, leading to enhanced particle settling. This strengthening of biological effects reduces the efficiency of physical resuspension even under comparable wind conditions, which results in the pronounced decline in SPM concentrations toward summer. The inverse seasonal patterns of Chl-a and SPM support this interpretation, aligning with previous studies that describe the role of phytoplankton in promoting flocculation and sedimentation in coastal systems. NN experiments suggest that calmer wind conditions alone can explain approximately ~40% of the observed summer SPM reduction compared to winter concentrations. Still, they do not account for up to ~80% decrease seen in the data. This substantial reduction is likely influenced by a variety of biologically related mechanisms, ranging from the microbial activity, production of EPS to zooplankton grazing. Further studies are needed to quantify the relative contributions of these individual mechanisms.

Overall, this study provides a comprehensive and quantitative assessment of how wind, tides, and biological activity interact to control SPM variability in a shallow, tidally dominated coastal system.

Conflict of Interest

The authors declare that they have no conflict of interest.

Author Contributions

GK performed the data analysis and wrote the initial draft of the manuscript. GK, VS, and AA carried out the numerical simulations. JvB, GK, and VS conceptualized the study. SH, SR, IK, and KHW contributed to the discussion of methods and interpretation of the results. All authors contributed to manuscript review and editing.

Data Availability

The source code of the FESOM-C model is publicly available via Zenodo: https://doi.org/10.5281/zenodo.2085177 (Androsov et al., 2018). The Sylt Roads observational dataset is accessible through the PANGAEA data portal: https://doi.org/10.1594/PANGAEA.873549, https://doi.org/10.1594/PANGAEA.873547, https://doi.org/10.1594/PANGAEA.918018, https://doi.org/10.1594/PANGAEA.918032, https://doi.org/10.1594/PANGAEA.918027, https://doi.org/10.1594/PANGAEA.918023, https://doi.org/10.1594/PANGAEA.918033, https://doi.org/10.1594/PANGAEA.918028, https://doi.org/10.1594/PANGAEA.918024, https://doi.org/10.1594/PANGAEA.918034, https://doi.org/10.1594/PANGAEA.918029, https://doi.org/10.1594/PANGAEA.918025, https://doi.org/10.1594/PANGAEA.918035, https://doi.org/10.1594/PANGAEA.918030, https://doi.org/10.1594/PANGAEA.918026, https://doi.org/10.1594/PANGAEA.918036, and https://doi.org/10.1594/PANGAEA.918031. Meteorological data, including hourly wind characteristics (station 3032, List auf Sylt; dataset ID: *urn:x wmo:md:de.dwd.cdc::obsgermany-climate-hourly-wind*) and daily sunshine duration (*urn:wmo:md:de-dwd-cdc:obsgermany-climate-daily-kl*), are available from the Climate Data Center (CDC) of the Deutscher Wetterdienst (DWD): https://opendata.dwd.de/climate_environment/. The Lagrangian model output and Neural Network results are available from the corresponding author upon reasonable request.

References

Aarup, T.: Transparency of the North Sea and Baltic Sea - a Secchi depth data mining study, Oceanologia, 44, 323–337, 2002.

775 Andersen, T. J.: The role of fecal pellets in sediment settling at an intertidal mudflat, the Danish
776 Wadden Sea, in: Proceedings in Marine Science, vol. 3, edited by: McAnally, W. H. and Mehta, A. J.,
777 Elsevier, 387–401, https://doi.org/10.1016/S1568-2692(00)80133-3, 2000.

778 Androsov, A., Fofonova, V., Kuznetsov, I., Danilov, S., Rakowsky, N., Harig, S., Holger, B., and
779 Wiltshire, K.H.: FESOM-C, , https://doi.org/10.5281/ZENODO.2085177, 2018.

780 Androsov, A., Fofonova, V., Kuznetsov, I., Danilov, S., Rakowsky, N., Harig, S., Brix, H., and
781 Wiltshire, K. H.: FESOM-C v.2: coastal dynamics on hybrid unstructured meshes, Geosci. Model Dev.,
782 12, 1009–1028, https://doi.org/10.5194/gmd-12-1009-2019, 2019.

783 Baird, D., Asmus, H., and Asmus, R.: Energy flow of a boreal intertidal ecosystem, the Sylt-Rømø
784 Bight, Mar. Ecol. Prog. Ser., 279, 45–61, https://doi.org/10.3354/meps279045, 2004.

785 Baird, D., Asmus, H., and Asmus, R.: Trophic dynamics of eight intertidal communities of the Sylt-
786 Rømø Bight ecosystem, northern Wadden Sea, Mar. Ecol. Prog. Ser., 351, 25–41,
787 https://doi.org/10.3354/meps07137, 2007.

788 Bale, A., Morris, A., and Howland, R.: Seasonal sediment movement in the Tamar Estuary,
789 Oceanologica Acta, 8, 1–6, 1985.

790 Bartholomä, A., Kubicki, A., Badewien, T. H., and Flemming, B. W.: Suspended sediment transport in
791 the German Wadden Sea—seasonal variations and extreme events, Ocean Dynamics, 59, 213–225,
792 https://doi.org/10.1007/s10236-009-0193-6, 2009.

793 Becherer, J., Flöser, G., Umlauf, L., and Burchard, H.: Estuarine circulation versus tidal pumping:
794 Sediment transport in a well-mixed tidal inlet, JGR Oceans, 121, 6251–6270,
795 https://doi.org/10.1002/2016JC011640, 2016.

796 Bruns, I., Bartholomä, A., Menjua, F., and Kopf, A.: Physical impact of bottom trawling on seafloor
797 sediments in the German North Sea, Front. Earth Sci., 11, 1233163,
798 https://doi.org/10.3389/feart.2023.1233163, 2023.

799 Burchard, H., Flöser, G., Staneva, J. V., Badewien, T. H., and Riethmüller, R.: Impact of Density
800 Gradients on Net Sediment Transport into the Wadden Sea, Journal of Physical Oceanography, 38, 566–
801 587, https://doi.org/10.1175/2007JPO3796.1, 2008.

802 Cadée, G. C.: Increased phytoplankton primary production in the Marsdiep area (Western Dutch
803 Wadden Sea), Netherlands Journal of Sea Research, 20, 285–290, https://doi.org/10.1016/0077-
804 7579(86)90050-5, 1986.

Christiansen, C., Vølund, G., Lund-Hansen, L. C., and Bartholdy, J.: Wind influence on tidal flat sediment dynamics: Field investigations in the Ho Bugt, Danish Wadden Sea, Marine Geology, 235, 75–86, https://doi.org/10.1016/j.margeo.2006.10.006, 2006.

Cloern, J. E.: Turbidity as a control on phytoplankton biomass and productivity in estuaries, Continental Shelf Research, 7, 1367–1381, https://doi.org/10.1016/0278-4343(87)90042-2, 1987.

Colijn, F.: Light absorption in the waters of the Ems-Dollard estuary and its consequences for the growth of phytoplankton and microphytobenthos, Netherlands Journal of Sea Research, 15, 196–216, https://doi.org/10.1016/0077-7579(82)90004-7, 1982.

de Jonge, V. N.: Relations Between Annual Dredging Activities, Suspended Matter Concentrations, and the Development of the Tidal Regime in the Ems Estuary, Can. J. Fish. Aquat. Sci., 40, s289–s300, https://doi.org/10.1139/f83-290, 1983.

de Jonge, V. N. and van Beusekom, J. E. E.: Wind- and tide-induced resuspension of sediment and microphytobenthos from tidal flats in the Ems estuary, Limnol. Oceanogr., 40, 776–778, https://doi.org/10.4319/lo.1995.40.4.0776, 1995.

de Jonge, V. N. and de Jong, D. J.: 'Global Change' Impact of Inter-Annual Variation in Water Discharge as a Driving Factor to Dredging and Spoil Disposal in the River Rhine System and of Turbidity in the Wadden Sea, Estuarine, Coastal and Shelf Science, 55, 969–991, https://doi.org/10.1006/ecss.2002.1039, 2002.

Depestele, J., Ivanović, A., Degrendele, K., Esmaeili, M., Polet, H., Roche, M., Summerbell, K., Teal, L. R., Vanelslander, B., and O'Neill, F. G.: Measuring and assessing the physical impact of beam trawling, ICES Journal of Marine Science, 73, i15–i26, https://doi.org/10.1093/icesjms/fsv056, 2016.

Dissanayake, D. M. P. K., Ranasinghe, R., and Roelvink, J. A.: The morphological response of large tidal inlet/basin systems to relative sea level rise, Climatic Change, 113, 253–276, https://doi.org/10.1007/s10584-012-0402-z, 2012.

Dolch, T. and Reise, K.: Long-term displacement of intertidal seagrass and mussel beds by expanding large sandy bedforms in the northern Wadden Sea, Journal of Sea Research, 63, 93–101, https://doi.org/10.1016/j.seares.2009.10.004, 2010.

Dronkers, J.: Tidal asymmetry and estuarine morphology, Netherlands Journal of Sea Research, 20, 117–131, https://doi.org/10.1016/0077-7579(86)90036-0, 1986.

Dyer, K. R.: Chapter 14 Sediment Transport Processes in Estuaries, in: Developments in Sedimentology, vol. 53, Elsevier, 423–449, https://doi.org/10.1016/S0070-4571(05)80034-2, 1995.

Egbert, G. D. and Erofeeva, S. Y.: Efficient Inverse Modeling of Barotropic Ocean Tides, J. Atmos. Oceanic Technol., 19, 183–204, https://doi.org/10.1175/1520-0426(2002)019<0183:EIMOBO>2.0.CO;2, 2002.

Eisma, D.: Flocculation and de-flocculation of suspended matter in estuaries, Netherlands Journal of Sea Research, 20, 183–199, https://doi.org/10.1016/0077-7579(86)90041-4, 1986.

Engel, A. and Schartau, M.: Influence of transparent exopolymer particles (TEP) on sinking velocity of Nitzschia closterium aggregates, Mar. Ecol. Prog. Ser., 182, 69–76, https://doi.org/10.3354/meps182069, 1999.

Fettweis, M., Monbaliu, J., Baeye, M., Nechad, B., and van Den Eynde, D.: Weather and climate induced spatial variability of surface suspended particulate matter concentration in the North Sea and the English Channel, Methods in Oceanography, 3–4, 25–39, https://doi.org/10.1016/j.mio.2012.11.001, 2012.

Flöser, G., Burchard, H., and Riethmüller, R.: Observational evidence for estuarine circulation in the German Wadden Sea, Continental Shelf Research, 31, 1633–1639, https://doi.org/10.1016/j.csr.2011.03.014, 2011.

Fofonova, V., Androsov, A., Sander, L., Kuznetsov, I., Amorim, F., Hass, H. C., and Wiltshire, K. H.: Non-linear aspects of the tidal dynamics in the Sylt-Rømø Bight, south-eastern North Sea, Ocean Sci., 15, 1761–1782, https://doi.org/10.5194/os-15-1761-2019, 2019.

Friedrichs, C. T. and Aubrey, D. G.: Non-linear tidal distortion in shallow well-mixed estuaries: a synthesis, Estuarine, Coastal and Shelf Science, 27, 521–545, https://doi.org/10.1016/0272-7714(88)90082-0, 1988.

Friedrichs, C. and Perry, J.: Tidal salt marsh morphodynamics: a synthesis, Journal of Coastal Research, 27, 7–37, 2001.

Graf, G. and Rosenberg, R.: Bioresuspension and biodeposition: a review, Journal of Marine Systems, 11, 269–278, https://doi.org/10.1016/S0924-7963(96)00126-1, 1997.

Hagen, R., Winter, C., and Kösters, F.: Changes in tidal asymmetry in the German Wadden Sea, Ocean Dynamics, 72, 325–340, https://doi.org/10.1007/s10236-022-01509-9, 2022.

Hommersom, A., Peters, S., Wernand, M. R., and de Boer, J.: Spatial and temporal variability in bio-optical properties of the Wadden Sea, Estuarine, Coastal and Shelf Science, 83, 360–370, https://doi.org/10.1016/j.ecss.2009.03.042, 2009.

Jansen, H., van Den Bogaart, L., Hommersom, A., and Capelle, J.: Spatio-temporal analysis of sediment plumes formed by mussel fisheries and aquaculture in the western Wadden Sea, Aquacult. Environ. Interact., 15, 145–159, https://doi.org/10.3354/aei00458, 2023.

Jeffrey, S. W. and Humphrey, G. F.: New spectrophotometric equations for determining chlorophylls a, b, c1 and c2 in higher plants, algae and natural phytoplankton, Biochemie und Physiologie der Pflanzen, 167, 191–194, https://doi.org/10.1016/S0015-3796(17)30778-3, 1975.

Jung, A., van Der Veer, H., Philippart, C., Waser, A., Ens, B., de Jonge, V., and Schückel, U.: Impacts of macrozoobenthic invasions on a temperate coastal food web, Mar. Ecol. Prog. Ser., 653, 19–39, https://doi.org/10.3354/meps13499, 2020.

Konyssova, G., Sidorenko, V., Androsov, A., Sander, L., Danilov, S., Rubinetti, S., Burchard, H., Winter, C., Wiltshire, K.H.: Changes in tidal dynamics in response to sea level rise in the Sylt-Rømø Bight (Wadden Sea), Ocean Dynamics, 75, 43, https://doi.org/10.1007/s10236-025-01688-1, 2025.

Kuznetsov, I., Androsov, A., Fofonova, V., Danilov, S., Rakowsky, N., Harig, S., and Wiltshire, K. H.: Evaluation and Application of Newly Designed Finite Volume Coastal Model FESOM-C, Effect of Variable Resolution in the Southeastern North Sea, Water, 12, 1412, https://doi.org/10.3390/w12051412, 2020.

Kuznetsov, I., Rabe, B., Androsov, A., Fang, Y.-C., Hoppmann, M., Quintanilla-Zurita, A., Harig, S., Tippenhauer, S., Schulz, K., Mohrholz, V., Fer, I., Fofonova, V., and Janout, M.: Dynamical reconstruction of the upper-ocean state in the central Arctic during the winter period of the MOSAiC expedition, Ocean Sci., 20, 759–777, https://doi.org/10.5194/os-20-759-2024, 2024.

Lettmann, K. A., Wolff, J.-O., and Badewien, T. H.: Modeling the impact of wind and waves on suspended particulate matter fluxes in the East Frisian Wadden Sea (southern North Sea), Ocean Dynamics, 59, 239–262, https://doi.org/10.1007/s10236-009-0194-5, 2009.

Loebl, M., Dolch, T., and van Beusekom, J. E. E.: Annual dynamics of pelagic primary production and respiration in a shallow coastal basin, Journal of Sea Research, 58, 269–282, https://doi.org/10.1016/j.seares.2007.06.003, 2007.

Lunau, M., Lemke, A., Dellwig, O., and Simon, M.: Physical and biogeochemical controls of microaggregate dynamics in a tidally affected coastal ecosystem, Limnol. Oceanogr., 51, 847–859, https://doi.org/10.4319/lo.2006.51.2.0847, 2006.

Maerz, J., Hofmeister, R., van Der Lee, E. M., Gräwe, U., Riethmüller, R., and Wirtz, K. W.: Maximum sinking velocities of suspended particulate matter in a coastal transition zone, Biogeosciences, 13, 4863–4876, https://doi.org/10.5194/bg-13-4863-2016, 2016.

Maerz, J. and Wirtz, K.: Resolving physically and biologically driven suspended particulate matter dynamics in a tidal basin with a distribution-based model, Estuarine, Coastal and Shelf Science, 84, 128–138, https://doi.org/10.1016/j.ecss.2009.05.015, 2009.

Neder, C., Fofonova, V., Androsov, A., Kuznetsov, I., Abele, D., Falk, U., Schloss, I. R., Sahade, R., and Jerosch, K.: Modelling suspended particulate matter dynamics at an Antarctic fjord impacted by glacier melt, Journal of Marine Systems, 231, 103734, https://doi.org/10.1016/j.jmarsys.2022.103734, 2022.

Passow, U.: Transparent exopolymer particles (TEP) in aquatic environments, Progress in Oceanography, 55, 287–333, https://doi.org/10.1016/S0079-6611(02)00138-6, 2002.

Pawlowicz, R., Beardsley, B., and Lentz, S.: Classical tidal harmonic analysis including error estimates in MATLAB using T_TIDE, Computers & Geosciences, 28, 929–937, https://doi.org/10.1016/S0098-3004(02)00013-4, 2002.

Postma, H.: Sediment transport and sedimentation in the estuarine environment, American Association of Advanced Sciences, 83, 158–179, 1967.

Postma, H.: Exchange of materials between the North Sea and the Wadden Sea, Marine Geology, 40, 199–213, https://doi.org/10.1016/0025-3227(81)90050-5, 1981.

Purkiani, K., Becherer, J., Flöser, G., Gräwe, U., Mohrholz, V., Schuttelaars, H. M., and Burchard, H.: Numerical analysis of stratification and destratification processes in a tidally energetic inlet with an ebb tidal delta, J. Geophys. Res. Oceans, 120, 225–243, https://doi.org/10.1002/2014JC010325, 2015.

Rick, J. J., Scharfe, M., Romanova, T., van Beusekom, J. E. E., Asmus, R., Asmus, H., Mielck, F., Kamp, A., Sieger, R., and Wiltshire, K. H.: An evaluation of long-term physical and hydrochemical measurements at the Sylt Roads Marine Observatory (1973–2019), Wadden Sea, North Sea, Earth Syst. Sci. Data, 15, 1037–1057, https://doi.org/10.5194/essd-15-1037-2023, 2023.

Rubinetti, S., Fofonova, V., Arnone, E., and Wiltshire, K. H.: A Complete 60-Year Catalog of Wind Events in the German Bight (North Sea) Derived From ERA5 Reanalysis Data, Earth and Space Science, 10, e2023EA003020, https://doi.org/10.1029/2023EA003020, 2023.

Schartau, M., Riethmüller, R., Flöser, G., van Beusekom, J. E. E., Krasemann, H., Hofmeister, R., and Wirtz, K.: On the separation between inorganic and organic fractions of suspended matter in a marine coastal environment, Progress in Oceanography, 171, 231–250, https://doi.org/10.1016/j.pocean.2018.12.011, 2019.

Sidorenko, V., Rubinetti, S., Akimova, A., Pogoda, B., Androsov, A., Beng, K. C., Sell, A. F., Pineda-Metz, S. E. A., Wegner, K. M., Brand, S. C., Shama, L. N. S., Wollschläger, J., Klemm, K., Rahdarian, A., Winter, C., Badewien, T., Kuznetsov, I., Herrling, G., Laakmann, S., and Wiltshire, K. H.:

Connectivity and larval drift across marine protected areas in the German bight, North Sea: Necessity of stepping stones, Journal of Sea Research, 204, 102563, https://doi.org/10.1016/j.seares.2025.102563, 2025.

Skogen, M., Ji, R., Akimova, A., Daewel, U., Hansen, C., Hjøllo, S., van Leeuwen, S., Maar, M., Macias, D., Mousing, E., Almroth-Rosell, E., Sailley, S., Spence, M., Troost, T., and van de Wolfshaar, K.: Disclosing the truth: Are models better than observations?, Mar. Ecol. Prog. Ser., 680, 7–13, https://doi.org/10.3354/meps13574, 2021.

Sprong, P. A. A., Fofonova, V., Wiltshire, K. H., Neuhaus, S., Ludwichowski, K. U., Käse, L., Androsov, A., and Metfies, K.: Spatial dynamics of eukaryotic microbial communities in the German Bight, Journal of Sea Research, 163, 101914, https://doi.org/10.1016/j.seares.2020.101914, 2020.

Stal, L. J.: Microphytobenthos as a biogeomorphological force in intertidal sediment stabilization, Ecological Engineering, 36, 236–245, https://doi.org/10.1016/j.ecoleng.2008.12.032, 2010.

Toullec, J., Vincent, D., Frohn, L., Miner, P., Le Goff, M., Devesa, J., and Moriceau, B.: Copepod Grazing Influences Diatom Aggregation and Particle Dynamics, Front. Mar. Sci., 6, 751, https://doi.org/10.3389/fmars.2019.00751, 2019.

Turner, J.: Zooplankton fecal pellets, marine snow and sinking phytoplankton blooms, Aquat. Microb. Ecol., 27, 57–102, https://doi.org/10.3354/ame027057, 2002.

van Beusekom, J. E. E. and de Jonge, V. N.: Long-term changes in Wadden Sea nutrient cycles: importance of organic matter import from the North Sea, in: Nutrients and Eutrophication in Estuaries and Coastal Waters, edited by: Orive, E., Elliott, M., and de Jonge, V. N., Springer Netherlands, Dordrecht, 185–194, https://doi.org/10.1007/978-94-017-2464-7_15, 2002.

van Beusekom, J. E. E., Brockmann, U. H., Hesse, K.-J., Hickel, W., Poremba, K., and Tillmann, U.: The importance of sediments in the transformation and turnover of nutrients and organic matter in the Wadden Sea and German Bight, Deutsche Hydrographische Zeitschrift, 51, 245–266, https://doi.org/10.1007/BF02764176, 1999.

van Maren, D. S., van Kessel, T., Cronin, K., and Sittoni, L.: The impact of channel deepening and dredging on estuarine sediment concentration, Continental Shelf Research, 95, 1–14, https://doi.org/10.1016/j.csr.2014.12.010, 2015.

Verney, R., Lafite, R., and Brun-Cottan, J.-C.: Flocculation Potential of Estuarine Particles: The Importance of Environmental Factors and of the Spatial and Seasonal Variability of Suspended Particulate Matter, Estuaries and Coasts, 32, 678–693, https://doi.org/10.1007/s12237-009-9160-1, 2009.

963   Winterwerp, J. C.: Stratification effects by cohesive and noncohesive sediment, J. Geophys. Res., 106,
964   22559–22574, https://doi.org/10.1029/2000JC000435, 2001.

965   Wotton, R.: The Essential Role of Exopolymers (Eps) in Aquatic Systems, in: Oceanography and
966   Marine Biology, vol. 20042243, edited by: Gibson, R., Atkinson, R., and Gordon, J., CRC Press, 57–94,
967   https://doi.org/10.1201/9780203507810.ch3, 2004.